

Neuromorphic control of embodied central pattern generators

A neuromorphological approach to motion

Christian Fernandez Lorden



Supervisors :

Pierre Sacré

Guillaume Drion

Thesis presented for obtaining the Master's degree in
Electrical engineering

University of Liege
Faculty of Applied Science
Academic Year 2022-2023

Neuromorphic control of embodied central pattern generators

A neuromorphological approach to motion

Christian Fernandez Lorden

Abstract

 Lorem ipsum dolor...

Contents

1	Introduction	5
2	Neurons and CPGs	7
2.1	Excitability	7
2.2	Conductance-based neuron models	8
2.3	Neuronal Behavior Metrics	10
2.4	Central Pattern Generators and Rhythms	11
2.5	Embodied Intelligence and CPGs	12
3	Modeling and analysis of neuronal circuits.	14
3.1	ODEs of the Neuronal Model	14
3.2	Behavior of neuron in function of its parameters	16
3.3	Bursting neuron characteristics	19
3.3.1	Spike number modulation with g_{s-}	19
3.3.2	Inter-burst frequency modulation with g_{p+}	20
3.4	Tonic spiking type-I neuron characteristics	21
3.5	ODEs of the synaptic connections	22
3.6	Half center oscillator analysis	23
4	A neuromorphic sensorimotor loop for pendulum swing	27
4.1	The mechanical system	27
4.2	Sensory feedback types	28
4.2.1	Angle based feedback	28
4.2.2	Angle and angular velocity based feedback	29
4.2.3	Spike based feedback	29
4.3	Controller with single motor neuron	31
4.3.1	Performance of the sensorimotor loop	31
4.3.2	Robustness of the sensorimotor loop	37
4.4	Two neuron "push-pull" controller	41
4.4.1	Performance of the sensorimotor loop	42
4.4.2	Robustness of the sensorimotor loop	43
5	Neuromodulation for adaptive amplitude control	49
5.1	Design of the controller	49
5.2	Controller performance	51

5.2.1	Static	51
5.2.2	Dynamic	51
5.3	Robustness analysis	51
6	Conclusion	56
A	Signal Analysis Algorithms	59

Chapter 1

Introduction

The control of robotic locomotion poses important challenges. In particular, we are still very far from achieving in robotic locomotion control with the same degree of robustness and adaptability to unexpected environmental perturbations exhibited by moving biological systems.

Also, the mobile nature of robots forces them to use batteries to power themselves. But, this creates an enormous problem, the battery limits the power that can be allocated to on-board computing. Yet, the state of the art in artificial intelligence nowadays is Deep Learning and it requires a lot of computing power to work well. This leads to two unsatisfactory solutions. Either get state of the art control, but dissociate the computing from the robot or drastically limit the robot autonomy. Or uses simpler methods that give poorer results but can be computed on-board.

To solve this energy problem, new approaches are emerging. One of them is neuromorphic engineering which aims to extract the useful properties of biological neuronal system to create highly efficient artificial neuronal controller or computing unit.

Indeed, the human brain is an incredibly energy-efficient processor. It is capable of simultaneously processing audio, visual and other sensory feedback while making decision on the future based on incomplete knowledge. To reuse an somewhat old but striking example, in 2016 AlphaGO bested one of the best human go player. Yet, AlphaGO consumed around 1 MW to accomplish this feat while the brain of Lee Sedol, the human player, only consumed around 20 W. And, in addition to playing the game, Lee's brain also processed all its sensory inputs, controlled its arm to make the moves on the board and continued regulating the equilibrium of its body. Better yet, after the game, he was able to go home and perform activities that are fundamentally different from playing go.

This energy gap between machine and human is explained by the fundamental difference in their computational architecture. The traditional architecture uses synchronized computing steps with memory separated from the computing. Conversely, in a neuronal net, the computing is done completely asynchronously and the memory of the systems is integrated in the computing since it is represented by the dynamical nature of the neurons.

In accordance with the limitations laid earlier, the goal of this thesis is to create and analyses a artificial neuronal controller capable of regulating the oscillation of a simple pendulum. The generated oscillation needs to be regular and the amplitude of this motion should be dynamically controllable using an external parameter.

Furthermore, the control architecture should be able to be interconnected to create a network of pendulums oscillation with different gaits.

Traditionally, control of such a system would be achieved through a PID using trajectory tracking or other simple continuous controllers. Those controllers often work in very restrained pendulum size spaces and need additional controllers to achieve gaits between multiple pendulums.

In this thesis, I will first define and explain some key neuromorphic concepts that will permeate my entire work. Then, I will define and analyse the specific neuronal model I used. After that, I will analyse simple controller that need to be able to sustain a regular oscillation. To this model I will add neuromodulation to be able to control the amplitude of the oscillation. Finally I will study the interconnection of multiple controllers to achieve gait patterns.

Note that multiple parameters will be assigned units, these are for distinguishing the role of the parameters but they do not represent physical values.

Chapter 2

Neurons and CPGs

This thesis the concepts of neurons and central pattern generators (CPGs) will be widely used. Before diving into the design and results of the proposed controller a clear understanding of these and other related concepts must be reached.

2.1 Excitability

The first step in the comprehension of neuronal system is the concept of excitability. In the words of Sepulchre et al. [8], “Excitability is the property of a system to exhibit all-or-none response to pulse inputs”. In other words, the system exhibit nearly no response from pulses until the pulse amplitude crosses a certain threshold after which the system responds completely.

In figure 2.1, an example of an excitable behavior is displayed. As can be seen, a very small difference in the pulse amplitude resulted in a very different neuronal behavior. The lower pulse resulted in the output faithfully following the input while the output of the higher one exhibited a very different behavior with oscillation and peaks far above the input. This specific behavior is known as bursting and will be discussed later.

This kind of all-or-none is desired since the effective control of the oscillation of a pendulum requires a very all-or-nothing control input. Indeed the moment of actuation is very important when controlling a pendulum and actuating at a bad time can lead to very poor results. Still, in the words of Sepulchre et al. [8], “[Excitability] is instrumental in converting sensory signals into motor actions”.

To create an excitable system a localized positive feedback loop is necessary. Indeed, the switch between two different responses after the crossing of a threshold requires the activation of a positive feedback near the threshold. This feedback pushes the output of the system to generate the excitable event.

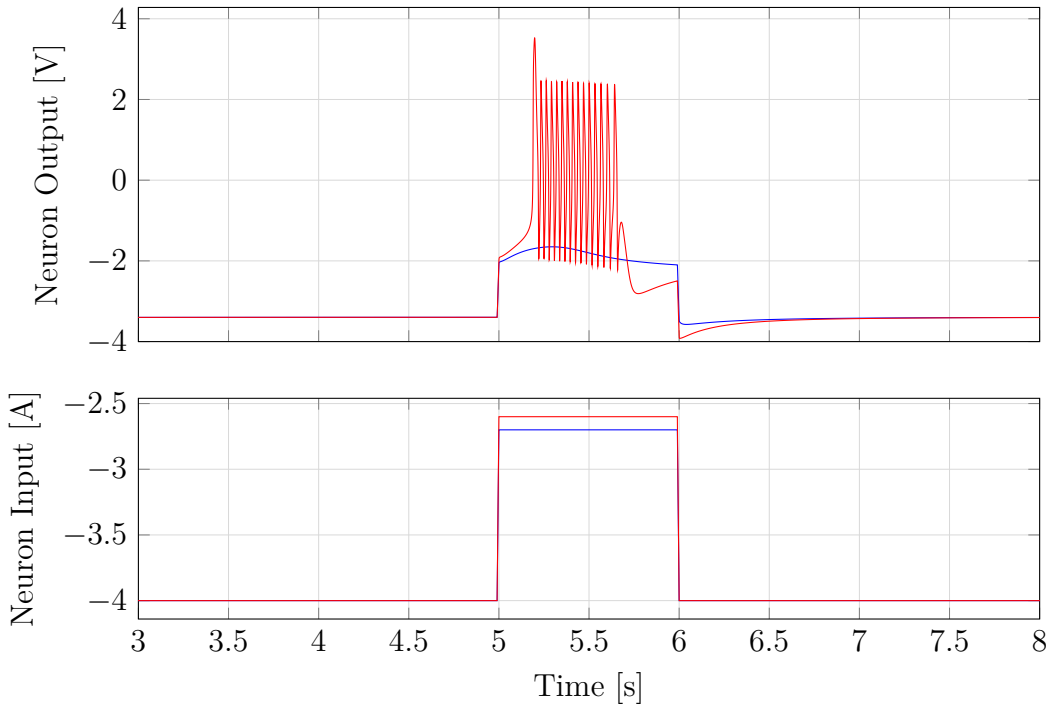


Figure 2.1: Example of an excitable behavior. Generated using neuron model of chapter 3.

2.2 Conductance-based neuron models

After having defined excitability, neuronal models can be understood more clearly. Indeed, neurons are a prime example of a excitable system.

Basically, neurons are cells that are able to receive input from the external world, send messages to one another and send motor commands to muscles. Since a neuron can be relatively big, it is evident that its behavior may be different at different part of the cell. But a common way to observe a neuron is to measure its activity in only one location.

As shown by Hodgkin et al. [4], the state of a neurons at its axon membrane is mostly dictated by ionic currents. In turn the state of the neuron influence the magnitude of those currents. This is illustrated on figure 2.2, where ionic currents are flowing through channels in the neuron membrane. Those channels activate and deactivate based on the membrane potential.

This language of ionic currents and membrane potential seems to designate classical circuit theory as a useful tool to model a neuron behavior. Hodgkin and Huxley [5] were the first to formulate a model of the neuronal behavior using a parallel network of varying conductances. Those conductances change based on the membrane voltage of the neuron at different rates. A classical representation of this model is seen in figure 2.3. On this diagram it can be seen that some ionic current discharge the capacity that represent the membrane while other charge it. Those charging current effectively act as positive feedback loops. Those are necessary for the excitable

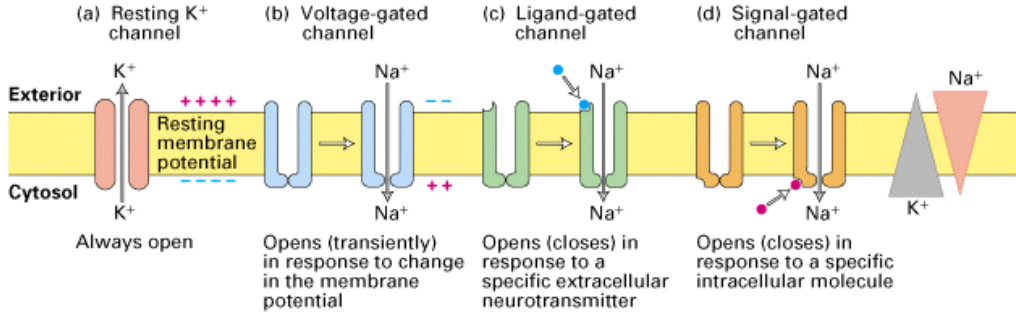


Figure 2.2: Simplified diagram of a biological neuron membrane. (Diagram taken from Lodish et al. [6])

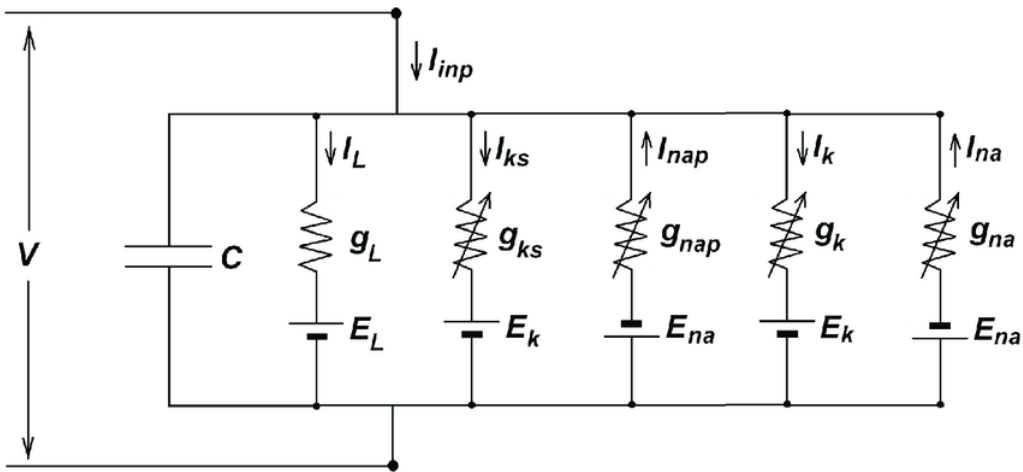


Figure 2.3: Simplified circuit of the neuron model. (Circuit taken from Vazifehkhah Ghaffari et al. [11])

behavior of a neuron.

This model can be written more formally using ordinary differential equation. Equations (2.1) to (2.5) are a general representation of this model. In this representation the i subscript denotes the different ionic currents that can be found in figure 2.3.

$$C \frac{\partial V}{\partial t} = I_{inp} - g_L (V - E_L) - \sum_i I_i \quad (2.1)$$

$$I_i(t, V) = g_i(t, V) (V - E_i) \quad (2.2)$$

$$g_i(t, V) = \bar{g}_i m_i(t, V)^p h_i(t, V)^q \quad (2.3)$$

$$\frac{\partial m_i(t, V)}{\partial t} = \frac{m_{i\infty}(V) - m_i(t, V)}{\tau_{mi}(V)} \quad (2.4)$$

$$\frac{\partial h_i(t, V)}{\partial t} = \frac{h_{i\infty}(V) - h_i(t, V)}{\tau_{hi}(V)} \quad (2.5)$$

The m_∞ and h_∞ terms follow a stretched and horizontally shifted sigmoid curve while the τ_m and τ_h terms follow a stretched and horizontally and vertically shifted sigmoid curve. The saturation of the ∞ terms shows that the ionic current feedbacks are localized in a certain range of membrane voltage.

This model is able to generate the whole range of neuronal behaviors seen in biological neuron. In this thesis, spiking and bursting, the two most common behaviors will be used. Those behaviors can be seen in figure 2.4. A spike is a sudden, short and steep increase in the neuron voltage followed by a sharp decrease and return to a resting voltage. A burst is the periodic apparition of a packet of spikes separated by periods of silence.

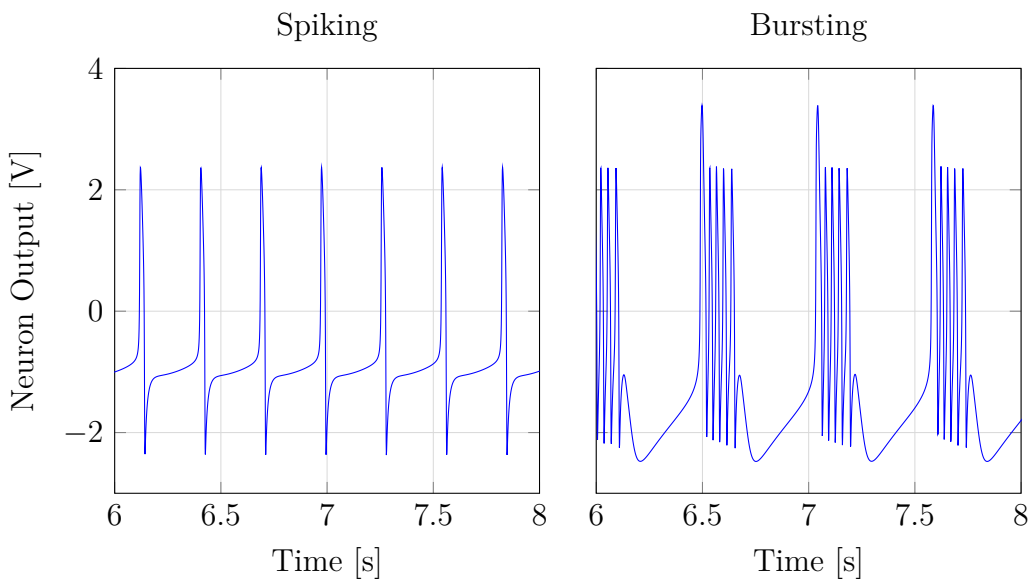


Figure 2.4: Example of spiking and bursting behaviors. Generated using neuron model of chapter 3.

2.3 Neuronal Behavior Metrics

To analyze and compare similar neuronal activities, multiple specific metrics are used. Here metrics to evaluate the tonic spiking and bursting will be discussed.

Figure 2.5 represents values that can be directly inferred from the trace of a tonic bursting neuron. Those values can be defined as

Burst length The average time of a burst event.

Rest length The average time of inactivity between two burst events.

Burst period The average time between the starts of two burst events.

Spike period Inside a burst, the average time between the starts of two spike events.

Number of spikes The average number of spike inside a burst event.

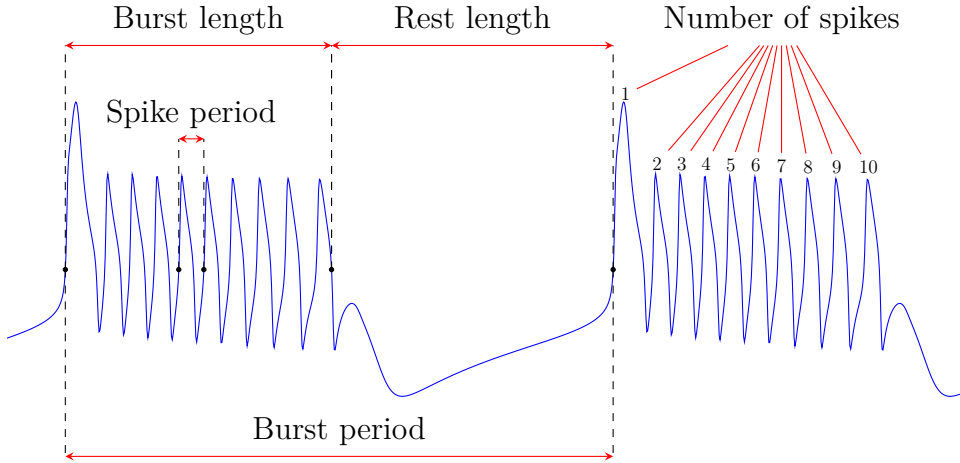


Figure 2.5: Illustration of the different metrics for bursting. Generated using neuron model of chapter 3.

Those raw metrics aside from the number of spikes, are not what is used in this thesis. Instead, the following set of metrics derived from the aforementioned values.

Inter-burst frequency $\frac{1}{\text{Burst period}}$, the frequency at which bursts occur.

Intra-burst frequency $\frac{1}{\text{Spike period}}$, frequency at which spikes occur inside a burst event.

Duty cycle $\frac{\text{Burst length}}{\text{Burst period}}$, the portion of time of the signal where the neuron is inside a burst event.

Number of spikes The average number of spike inside a burst event.

The tonic spiking does not require so much metrics. Simply measuring the **Spike period** is enough to compute the **Spiking frequency** which is the most useful metric to describe a spiking behavior.

2.4 Central Pattern Generators and Rhythms

To develop the controller, the concept of central pattern generators is very useful since they are linked closely to rhythmic movement. And, the oscillation of a pendulum is a naturally rhythmic movement.

From Straub [10], “A central pattern generator (CPG) is an assembly of neurons that possesses the ability to produce a rhythmic activity pattern without [] sensory feedback information”.

Also, it is widely admitted that central pattern generators are frequently found in biological motion systems. Marder and Bucher [7], Grillner [3] highlight that CPGs are abundant in the control of animals motion.

To keep it simple, the connections between neurons inside a CPG result in the activity of one neuron generating currents in the other neuron. Those connections can have two types, inhibitory and excitatory. An inhibitory connection results in negative current being injected while an excitatory connection creates a positive current.

The most simple and well studied CPG is the half-center oscillator [9]. This specific circuit is composed of two neurons that inhibit each other. The system along with simulation can be seen in 2.6.

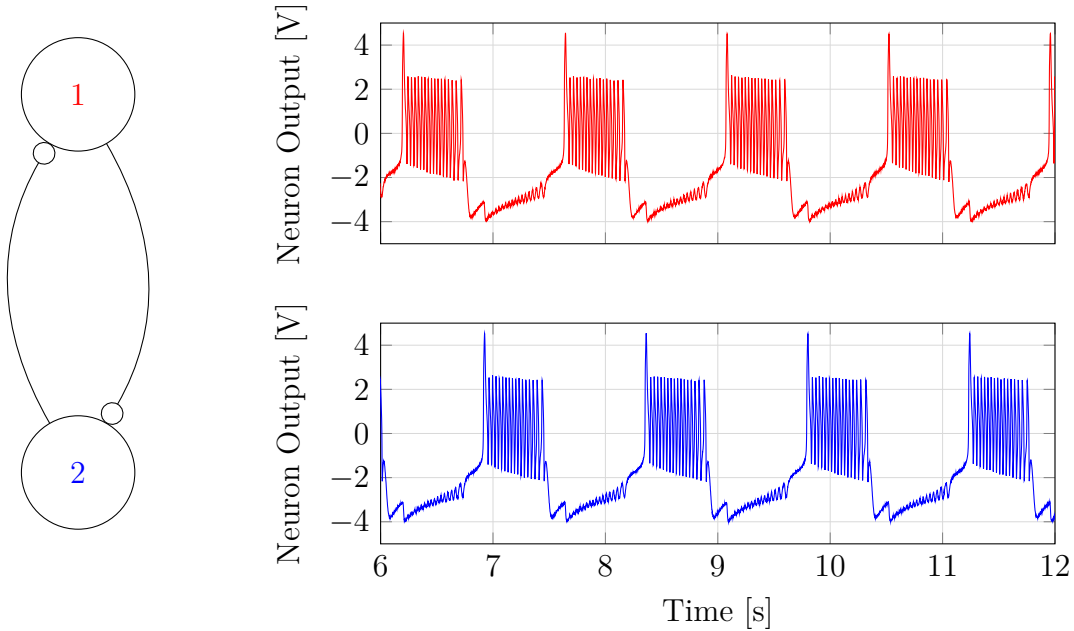


Figure 2.6: Example of an half center oscillator. Traces were generated using neuron model of chapter 3.

The generation of rhythmic patterns is clear when looking at the traces of the activation of the different neurons. Indeed, the activation of neuron 1 and neuron 2 always follow each other. This alternate can be expressed in term of phase by saying that one neuron has a phase of $\frac{1}{2}$ of a period compared to the other.

2.5 Embodied Intelligence and CPGs

From Cangelosi et al. [1] “Embodied intelligence is the computational approach to the design and understanding of intelligent behavior in embodied and situated agents through the consideration of the strict coupling between the agent and its environment (situatedness), mediated by the constraints of the agent’s own body, perceptual and motor system, and brain (embodiment).”

This concept is describing the goal of this thesis. Indeed , the model that is developed later is a prime example of embodied intelligence. The controller will process direct sensory input to generate coherent control signals for the motor. Using neuromodulation the strength of the push will be changed according to a desired amplitude.

More broadly, the concept of embodied intelligence is closely related to CPGs. Indeed, CPGs are circuits that are rhythmic without sensory feedback, but using sensory feedback to tune the frequency of the CPG to the external is thought to be inner working of most biological motion controller (citation needed). This coupling is precisely a low-level embodied intelligence.

Chapter 3

Modeling and analysis of neuronal circuits.

3.1 ODEs of the Neuronal Model

The backbone of the model I used is based on a model developed by A. Franci (use a citation maybe). A diagram of this model can be seen in figure 3.1. This diagram can be translated into ODEs, those ODE are the Equations (3.1) to (3.8).

$$\tau_o \frac{\partial V}{\partial t} = V_0 + I_a - i_{f-} - i_{s+} - i_{s-} - i_{u+} - V \quad (3.1)$$

$$i_{f-} = g_{f-} (\tanh(v_f - d_{f-}) - \tanh(V_0 - d_{f-})) \quad (3.2)$$

$$i_{s+} = g_{s+} (\tanh(v_s - d_{s+}) - \tanh(V_0 - d_{s+})) \quad (3.3)$$

$$i_{s-} = g_{s-} (\tanh(v_s - d_{s-}) - \tanh(V_0 - d_{s-})) \quad (3.4)$$

$$i_{u+} = g_{u+} (\tanh(v_u - d_{u+}) - \tanh(V_0 - d_{u+})) \quad (3.5)$$

$$\tau_f \frac{\partial v_f}{\partial t} = V - v_f \quad (3.6)$$

$$\tau_s \frac{\partial v_s}{\partial t} = V - v_s \quad (3.7)$$

$$\tau_u \frac{\partial v_u}{\partial t} = V - v_u \quad (3.8)$$

with $g_{f-}, g_{s-} < 0$, $g_{s+}, g_{u+} > 0$ and $d_{f-}, d_{s+}, d_{s-}, d_{u+} \in \mathbb{R}$.

Here i_{f-} is the fast positive feedback to the neuron, i_{s+} and i_{s-} are the slow negative and positive feedback and i_{u+} is the ultra-slow negative feedback.

i_{s+} and i_{s-} could be written as a single current, but, since they play a different role in the neuron behavior and to keep the symmetry between the currents they are written separately.

This model follows the findings of Franci et al. [2]. They state that a tunable and robust behavior must have a slow positive feedback. Slow in this context means in a timescale between the fast positive feedback that creates the spike and the ultra-slow feedback that slowly bring the neuron back to a resting voltage. Here the

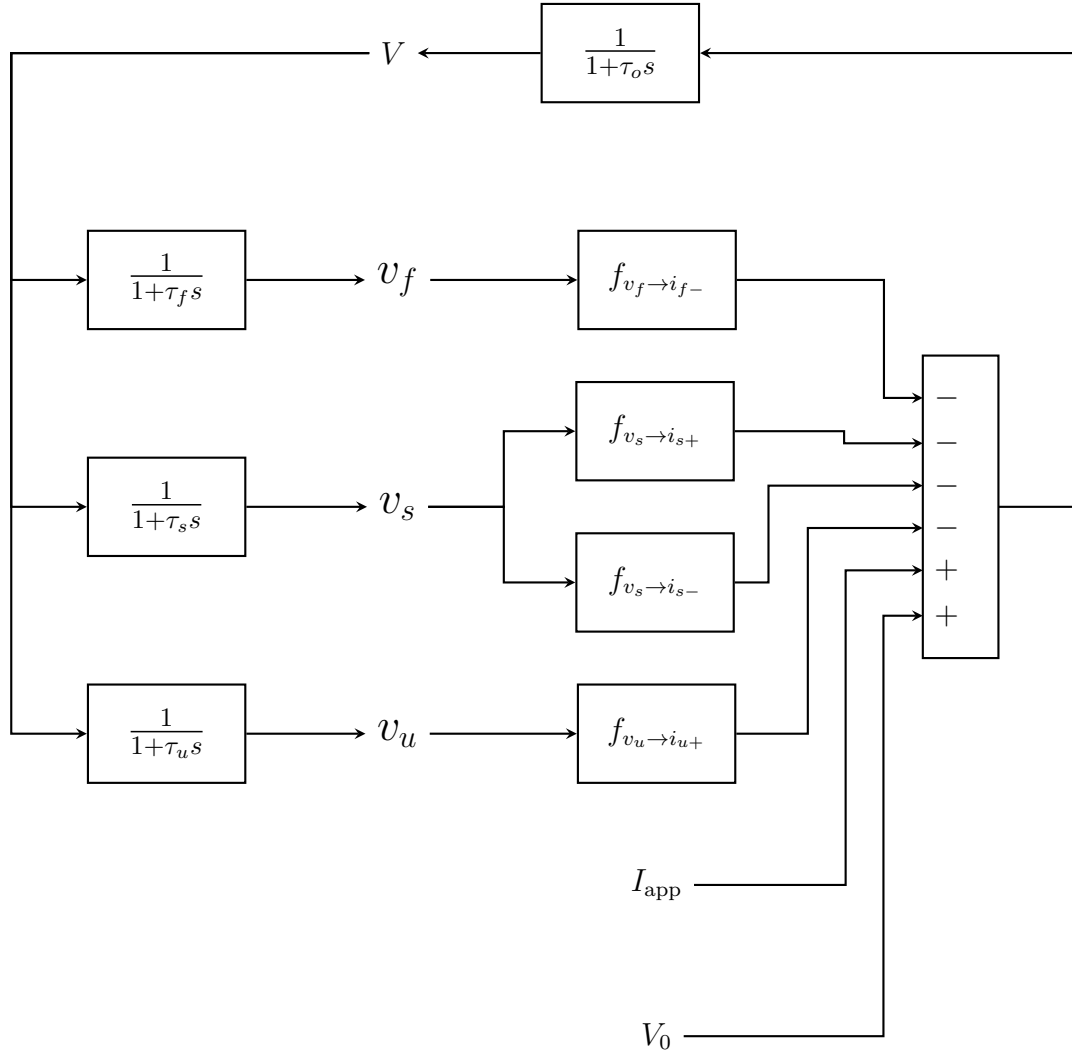


Figure 3.1: Diagram of the Neuron Model. The output of the neuron is V and the input is I_a .

i_{s-} currents fill this role. This lead to a model that is more stable to small changes in parameters.

For this thesis, some of the parameters of the model will remain fixed.

V_0	-0.85 V	τ_o	0.0004
d_{f-}	0.0 V	τ_f	0.001
d_{s+}	0.5 V	τ_s	0.04
d_{s-}	-0.5 V	τ_u	0.8
d_{u+}	-0.5 V		

In figure 3.2 a representation of all the currents and the voltages of the model is present.

The low-pass filter effect is very clear when looking at the different voltages. And the saturation of the current is very clear when seeing the flat regions of some

currents.

Furthermore, the "launching" effect of the slow positive feedback is very present, it very clearly is the first current to activate just before the burst and seems to "launch" it.

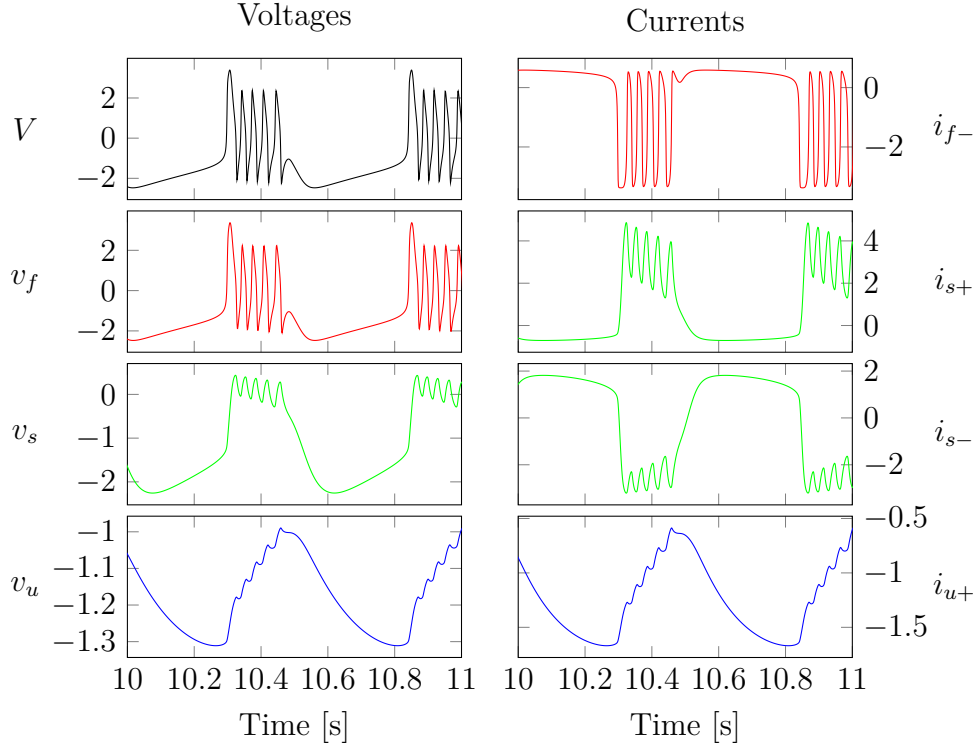


Figure 3.2: Currents and voltages inside the neuron model. The linked currents and voltages are color coded.

3.2 Behavior of neuron in function of its parameters

Before designing a controller, the behavior of this neuron must be studied to choose good parameters for the neuron. For this analysis only an exploration of the parameters g_{s-} , g_{u-} and I_{app} will be done.

Firstly, in figure 3.3, an overview of the different regions where the neuron is active.

For this thesis purposes the bursting region is the most interesting. The bursting region seems to advance until $I_{app} = 0.0$ then in recede back. It would seem that the parameters at the center of the chart are capable of sustaining bursting for a wide range of applied current. This thus seems to be the most interesting zone for the controller.

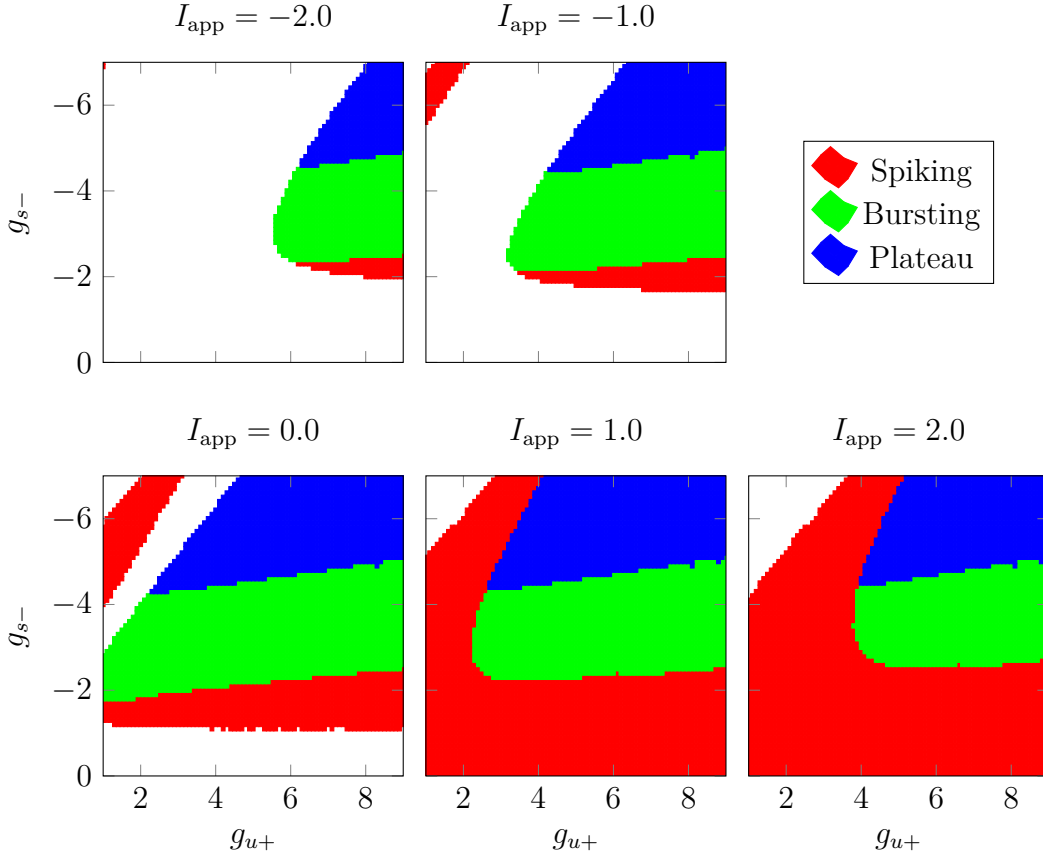


Figure 3.3: Map of the neuron activation types with $g_{f-} = -2.0$ and $g_{s+} = 6.0$. The plateau region correspond to bursting with a voltage plateau between the first spike and the rest.

Now that the good region has been seen, a closer look at the inter-burst frequency is useful. Indeed it is better to have neurons that are attuned to the frequency of the pendulum to get good results. In figure 3.4, it can be seen that the inter burst frequency is mostly decided by the conductances and not the applied current. Changing the applied current only change the "discovered" zone.

Yet by analyzing more closely, another zone of bursting can be discovered. In figure 3.5, those zones are highlighted. They happen in zones with next to no slow positive feedback. Yet, Franci et al. [2] indicates that the slow positive feedback is integral to a reliable bursting. This assertion can already be verified by how much the zone of bursting shift with a small change in input current. Yet, a more detailed analysis will be done to show the fragility of this bursting.

figure 3.6 reveals that the "fragile" burst is totally destabilized by the addition of a small noise. The regular 2 spike pattern ceases to exist and the number of spike per burst and the inter burst frequency seem to become very random. Yet the "stable" burst seems unaffected by the noise, the only way to see the noise is to look at the voltage during the resting period. The number of spikes and the inter burst frequency remains unchanged by the added noise.

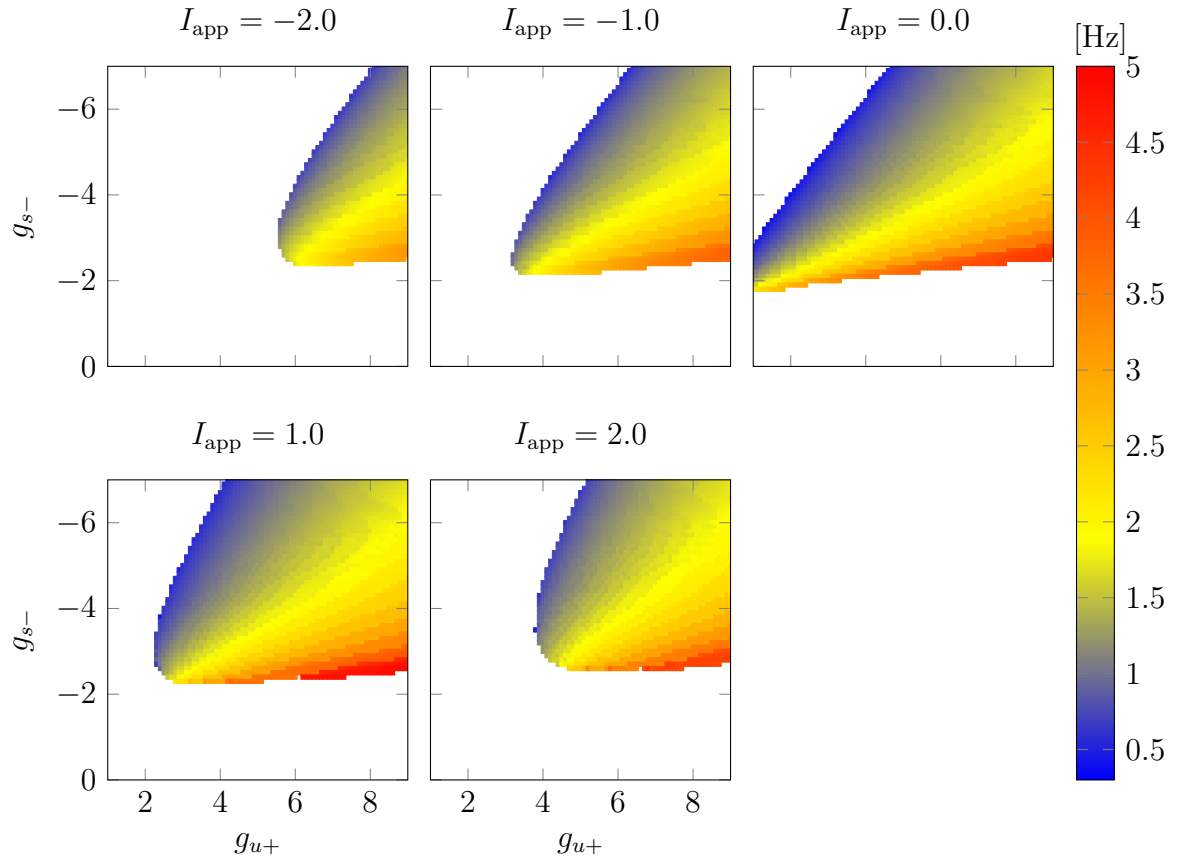
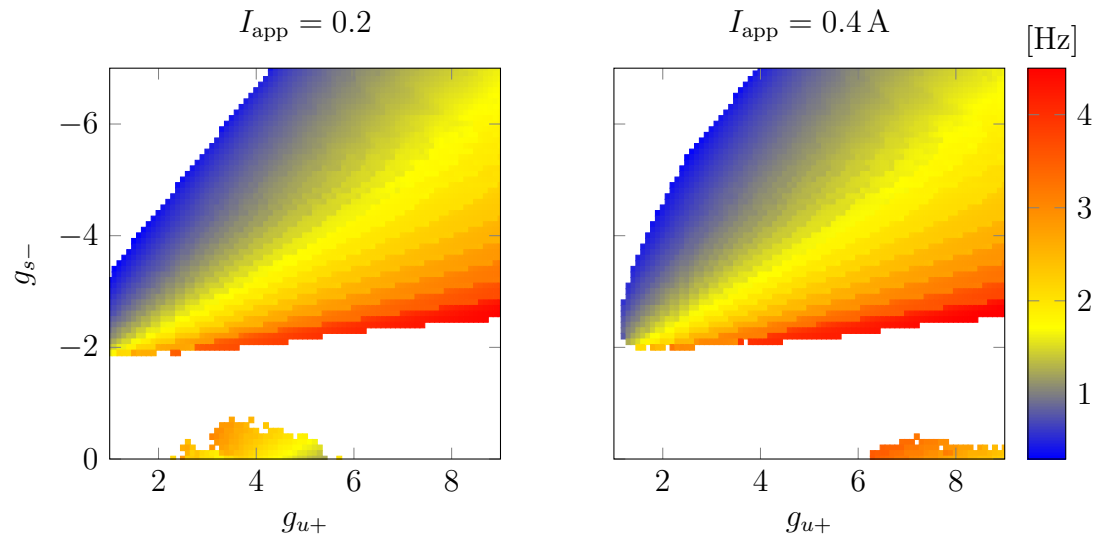


Figure 3.4: Neuron bursting frequency.

Figure 3.5: Neuron bursting frequency, zoom on some specific I_{app} . Apparitions of another bursting region.

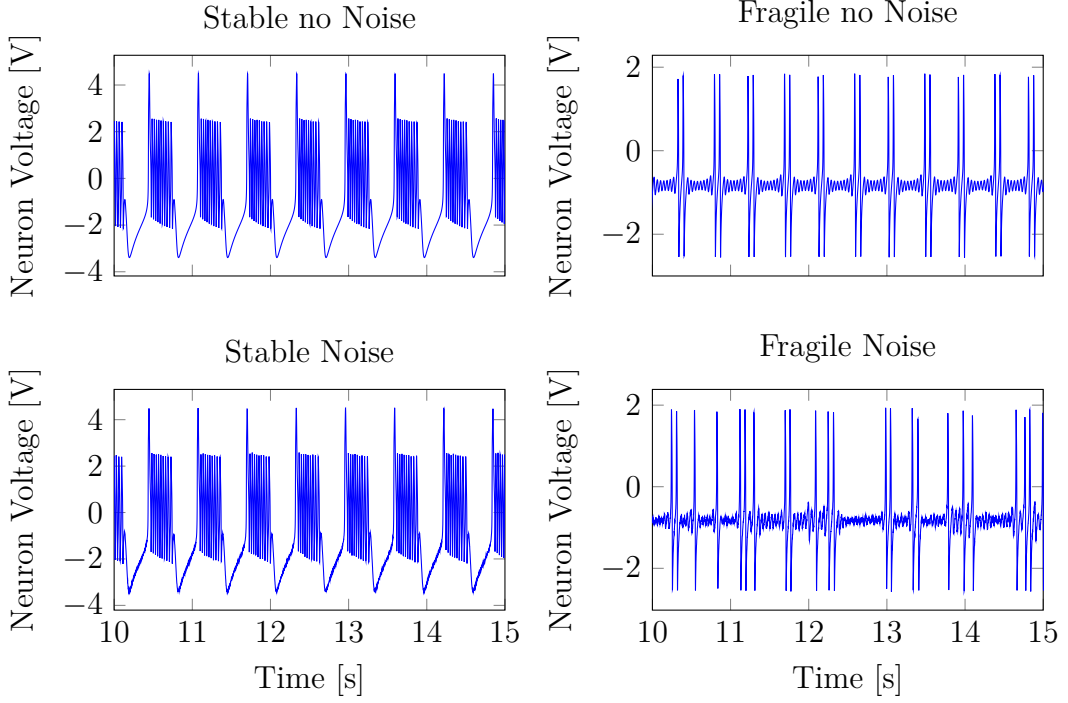


Figure 3.6: Comparison of both time of bursting at $I_{app} = 0.2 \text{ A}$. Stable model used $g_{s-} = -4$ and $g_{u+} = 5$ and fragile model used $g_{s-} = -0.2$ and $g_{u+} = 4$. The noise applied had a spectral power density of $n_{I_{app}} = 3 \times 10^{-7} \text{ V}^2 \text{ Hz}^{-1}$.

3.3 Bursting neuron characteristics

In this section the bursting behavior specifically will be studied. Some graph will only be done with one set of parameters for bursting but the conclusions draw will hold for all bursting in the region.

3.3.1 Spike number modulation with g_{s-}

A great way to change the amount of power transmitted by a burst is to change the number of spikes that are present in the burst. Indeed, if g_{f-} and g_{s+} are fixed, then the up time of a spike will remain nearly the same whatever the values of g_{s-} and g_{u+} are. This leads to the number of spike being the most important metric to characterize the power transmitted by the spikes.

Both g_{s-} and g_{u+} could be used to modulate the number of spikes. But, since figure 3.4 shows that the value of g_{u+} is more important when it comes to the existence of bursting, g_{s-} will be used as the parameter to modulate the number of spikes.

This modulation can be seen in figure 3.7. The graph shows a clear link between the number of spike in the burst and the g_{s-} parameter. The number of spike decreased "linearly" in as the amplitude of the feedback decreased.

Yet, to confirm that this metric was well correlated with the amount of power

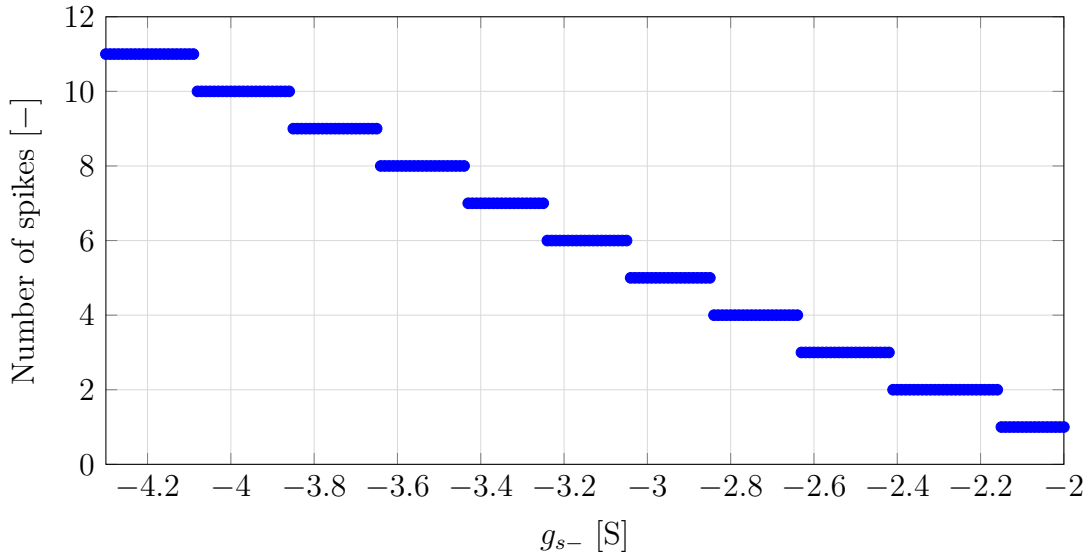


Figure 3.7: Curve of the number of spikes in function of the g_{s-} parameter. With $I_{\text{app}} = 1 \text{ A}$, $g_{f-} = -2 \text{ S}$, $g_{s+} = 6 \text{ S}$ and $g_{u+} = 5 \text{ S}$.

transmitted by the burst, a comparison with other metrics is necessary. In figure 3.8, the duty cycle and the mean positive value of the bursting are plotted. The mean positive value is defined as

$$\text{mean positive value} = \frac{1}{T} \int_{t_0}^{t_0+T} \max(0, V(t)) dt \quad (3.9)$$

This figure tells us that the number of spikes is indeed correlated with the power transmitted since the mean positive value is nearly constant with the number of spikes. But the duty cycle seems to be a poor indicator since it can have the same value in two very different cases.

The point of changing the power transmitted by the burst is integral in the control of the pendulum since it will be linked with the torque applied to the pendulum.

3.3.2 Inter-burst frequency modulation with g_{p+}

To get a reliable control, it is necessary that the natural frequency of the neuron is not too far away from the natural frequency of the pendulum.

Since g_{s-} is already used to change the power of a burst, g_{u+} will be used to modulate the inter-burst frequency. Figure 3.9 shows the influence of the parameter and the applied current on the inter-burst frequency. Interestingly, it seems that the bursting limit follows a linear relationship between I_{app} and g_{u+} in this model. The inter-burst frequency seems to be mostly dependent on g_{u+} when far away from the bursting boundary. Near the boundary the frequency is reduced compared to inside the boundary.

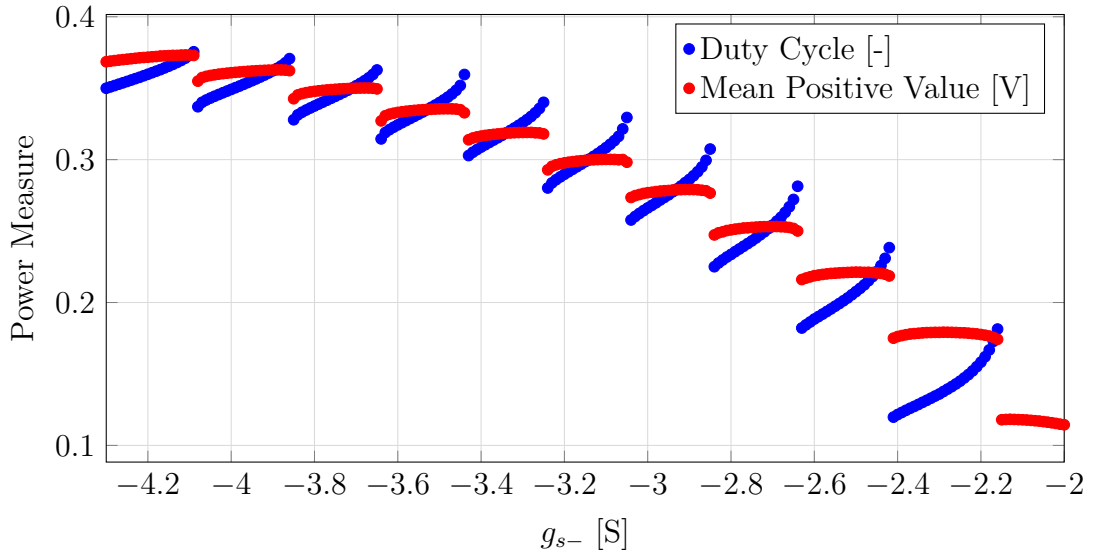


Figure 3.8: Curve of the burst power in function of the g_{s-} parameter. With $I_{app} = 1\text{ A}$, $g_{f-} = -2\text{ S}$, $g_{s+} = 6\text{ S}$ and $g_{u+} = 5\text{ S}$.

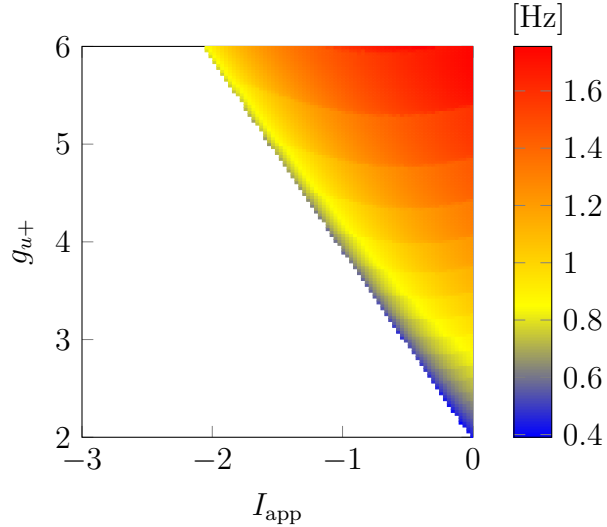


Figure 3.9: Map of the in function of the g_{u+} parameter. With $g_{f-} = -2\text{ S}$, $g_{s+} = 6\text{ S}$ and $g_{s-} = -4\text{ S}$.

3.4 Tonic spiking type-I neuron characteristics

For sensing purposes a tonic type-I spiking neuron will be useful. Such a neuron must be able to sustain spiking and have a spiking frequency that is closely correlated with the input current.

In figure 3.10, the firing frequency is plotted in function of the applied current. This figure clearly shows that for low values of applied current the spiking frequency is very strongly related with the input current. For higher currents the frequency

saturates and even decreases.

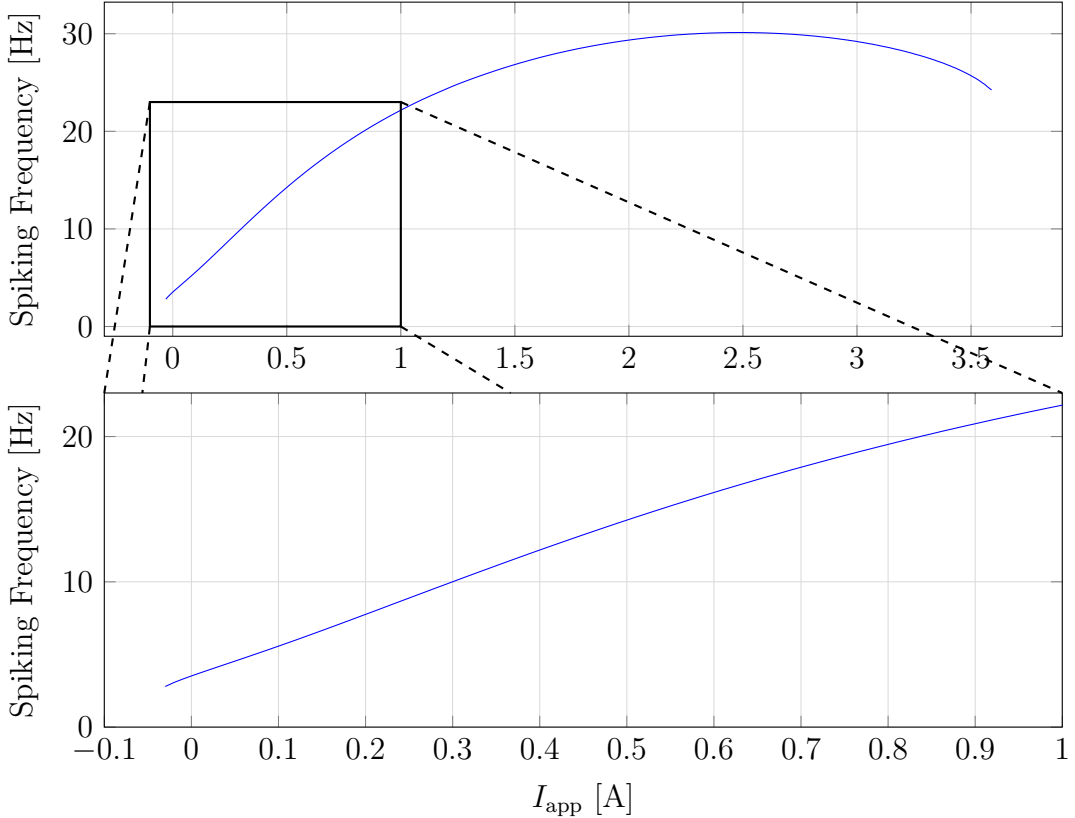


Figure 3.10: F-I curve of the type I neuron. With $g_{f-} = -2 \text{ S}$, $g_{s+} = 4 \text{ S}$, $g_{s-} = -1 \text{ S}$ and $g_{u+} = 1 \text{ S}$. The curve starts and ends at the beginning and end of spiking.

The correlation of the applied current with the spiking frequency is necessary to have a good representation of the input at the output of the neuron. In some way the neuron converts the amplitude of the input into a frequency.

3.5 ODEs of the synaptic connections

After the study of a single neuron, networks of neurons must be considered to find interesting behaviors. Biologically synapses are often found as inter-neurons connection. Figure 3.11 show the diagram of the synapse model that will be used in this thesis. It is composed of a low-pass filter followed by a non-linear voltage to current function. The synapse thus takes as input the voltage of a neuron a produces a current that can be fed as input to another neuron.

This model can be written more formally as an ODE.

$$\tau_{\text{syn}} \frac{\partial v_{\text{syn}}}{\partial t} = V - v_{\text{syn}} \quad (3.10)$$

$$i_{\text{out}} = g_{\text{syn}} \sigma(4(v_{\text{syn}} - d_{\text{syn}})) \quad (3.11)$$

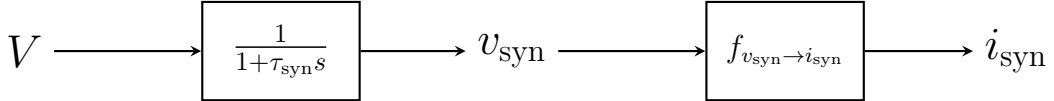


Figure 3.11: Diagram of the synapse Model. The output of the synapse is I_{out} and the input is V_{in} .

with $g_{\text{syn}}, d_{\text{syn}} \in \mathbb{R}$ and $\sigma()$ the sigmoid function.

The 4 factor inside the increases the slope of the sigmoid to get a faster transition.

Basically, when the input neuron is inactive its voltage is negative, thus the sigmoid function is nearly zero and no current is sent to the output neuron. And, when the neuron is active the sigmoid is non zero and might even saturate to 1 and a current is sent the output neuron. The sign of g_{syn} will decide if the synapse is excitatory or inhibitory. A negative conductance makes an inhibitory connection and a positive conductance makes an excitatory one.

3.6 Half center oscillator analysis

Formed by the interconnection of two neurons that are linked by two inhibitory synapses, the half-center oscillator (HCO) is a central component of the controller. A representation was already presented in chapter 2 by figure 2.6. Yet, a more detailed representation using specific parameters can be seen in figure 3.12.

The most interesting thing to study and control in the HCO is its frequency which can be evaluated by the inter-burst frequency of one of its neurons. Figure 3.13 depicts this frequency in function of I_{app} and g_{u+} for certain g_{syn} . Comparing with figure 3.9, low values of g_{syn} lead to behaviors very similar to uncoupled neurons while higher values lead to lower frequencies. The strength of the connection is thus very important for the behavior of the system.

To further show this, figure 3.14 represents the zones where bursting is caused by the network and not the intrinsic properties of the neurons. The higher the connection between the neurons is the larger the zone of bursting becomes.

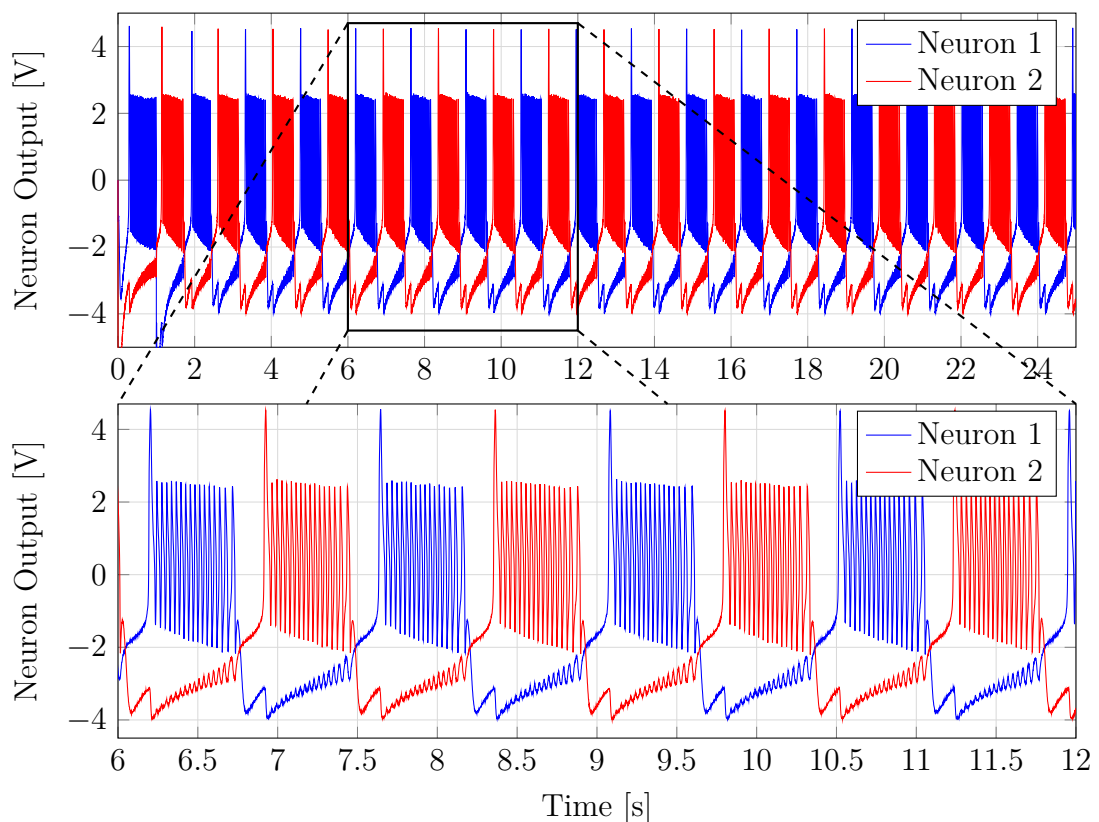


Figure 3.12: Plot of the neuronal output of a CPG. With $g_{f-} = -2 \text{ S}$, $g_{s+} = 6 \text{ S}$, $g_{s-} = -4 \text{ S}$, $g_{u+} = 3.7 \text{ S}$, $I_{\text{app}} = -1 \text{ A}$, $g_{\text{syn}} = -1 \text{ S}$ and $d_{\text{syn}} = 0 \text{ V}$.

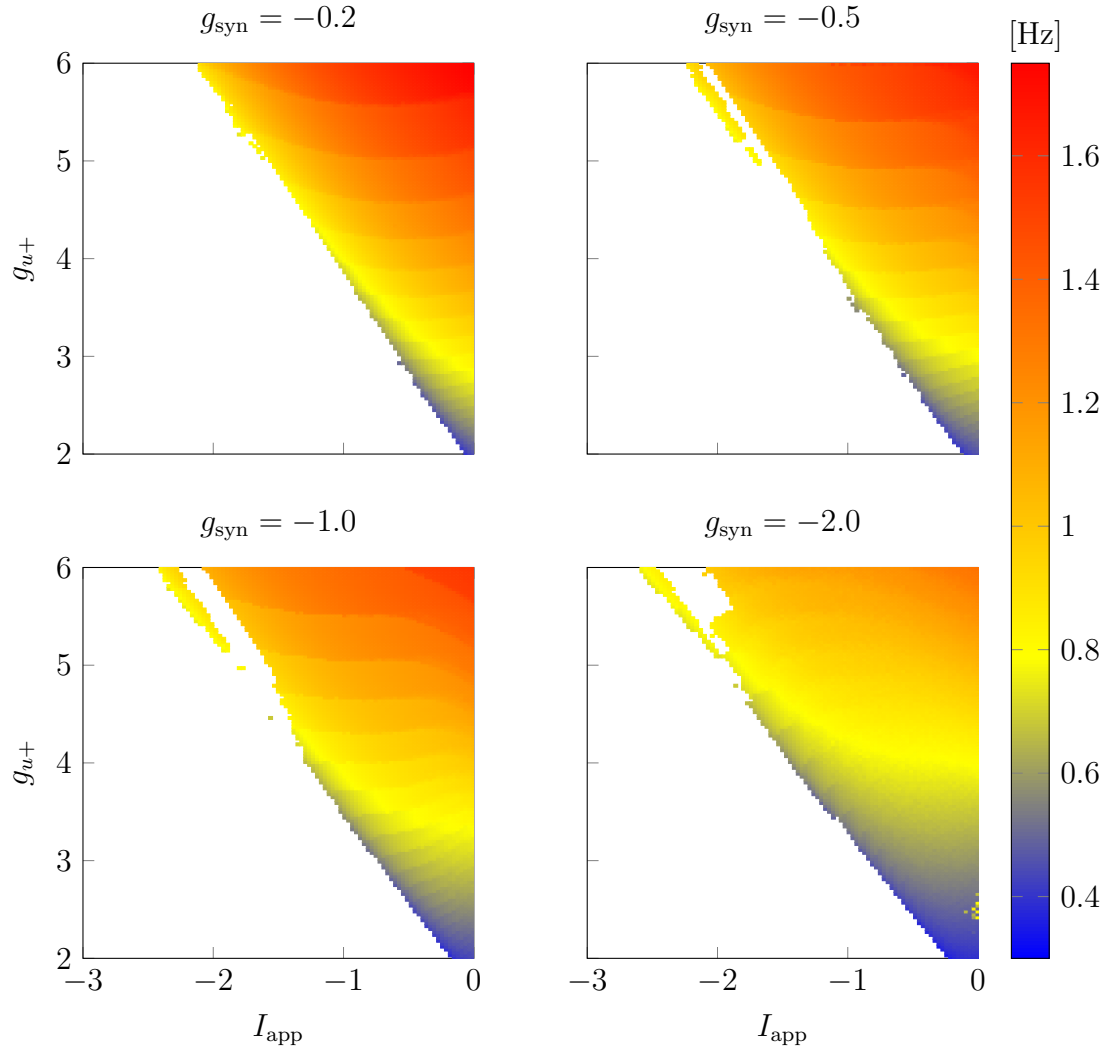


Figure 3.13: Activation of the cpg network in function of the ultra-slow negative feedback and the applied current. With $g_{f-} = -2 \text{ S}$, $g_{s+} = 6 \text{ S}$, $g_{s-} = -4 \text{ S}$ and $d_{\text{syn}} = 0 \text{ V}$.

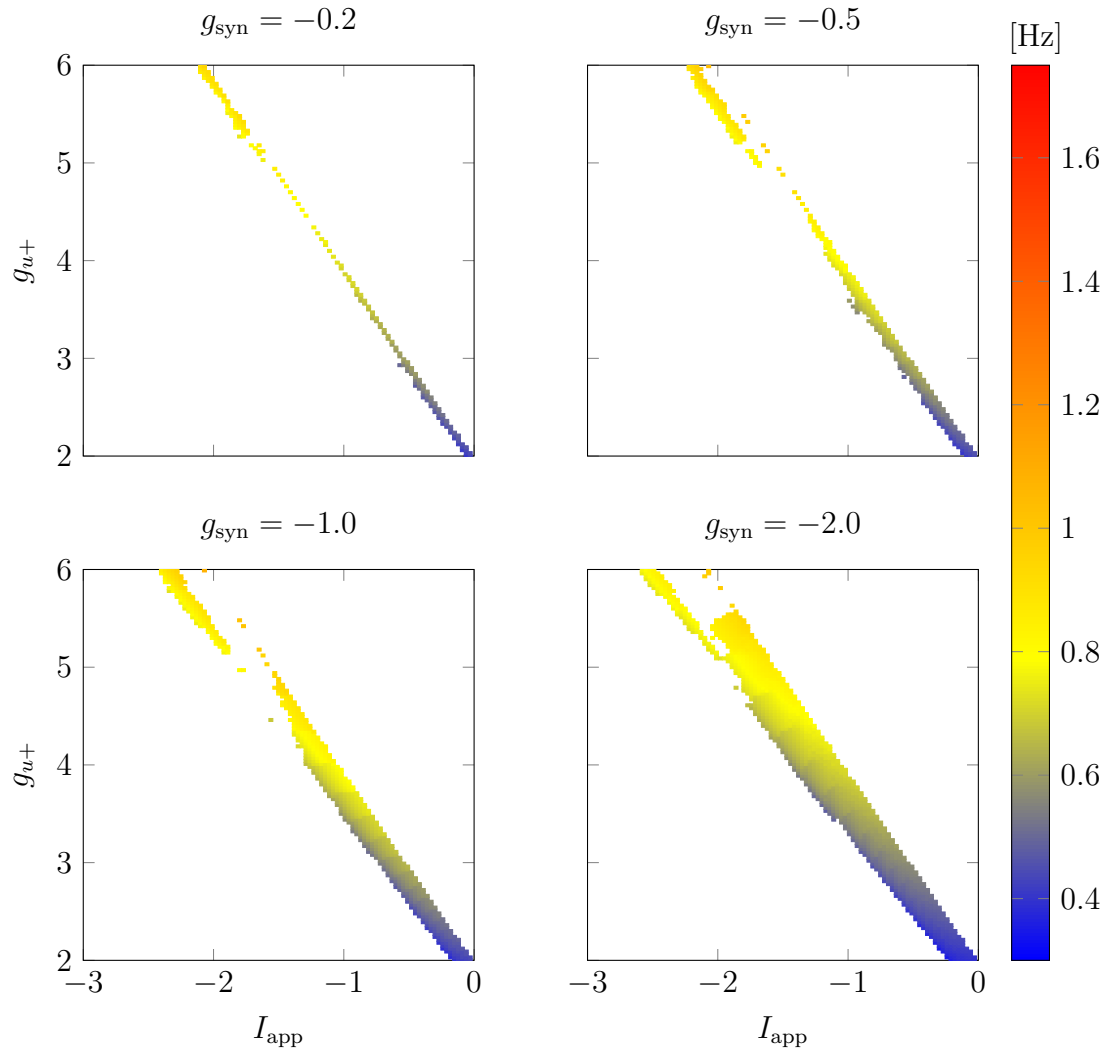


Figure 3.14: Activation of the cpg network in function of the ultra-slow negative feedback and the applied current. Only the region where the bursting only arise from the network is shown. With $g_{f-} = -2 \text{ S}$, $g_{s+} = 6 \text{ S}$, $g_{s-} = -4 \text{ S}$ and $d_{\text{syn}} = 0 \text{ V}$.

Chapter 4

A neuromorphic sensorimotor loop for pendulum swing

This section will focus on the control of a cylindrical pendulum with a neuromorphic controller. The primary goal of this section is to find and extract control schemes that are intrinsically linked with the mechanical. To reach this goal the different useful behaviors of the neuron model discussed in chapter 3 will be paired with multiple feedback models. The models will be evaluated for their performances and their robustness.

4.1 The mechanical system

Before diving into controller design, understanding the mechanical system is important. Figure 4.1 shows a graphical representation of the system. This shows that there is only a single control input to this system, the applied torque τ . The system also gives two meaningful state output, the angle θ with the vertical and the angular velocity $\dot{\theta}$. Finally the dynamics of the pendulum are influenced by 5 parameters, the radius r of the cylinder, the height h of the cylinder, the density ρ of the cylinder, the damping coefficient B_f which generates the friction torque τ_f at the rotation point and the gravity \mathbf{g} .

On the figure, the gray arrow shows and defines the down direction. It can be used to separate the rotation plane in two halves. The half with negative $\sin(\theta)$ and the half with positive $\sin(\theta)$.

For this controller the parameters of the pendulum will be kept mostly constant. Keeping the parameters in a certain close range is obviously necessary. A controller capable of stabilizing the oscillation of a 1 mm pendulum will struggle and fail when applied on a 1 m long pendulum. Keeping the values in same order of magnitude is necessary.

$$\begin{array}{lll} r & 0.05 \text{ m} & B_f \quad 0.01 \text{ N m s}^{\circ-1} = 0.57 \text{ N m s rad}^{-1} \\ h & 0.5 \text{ m} & \mathbf{g} \quad 9.81 \text{ m s}^{-2} \\ \rho & 1000 \text{ kg m}^{-3} & \end{array}$$

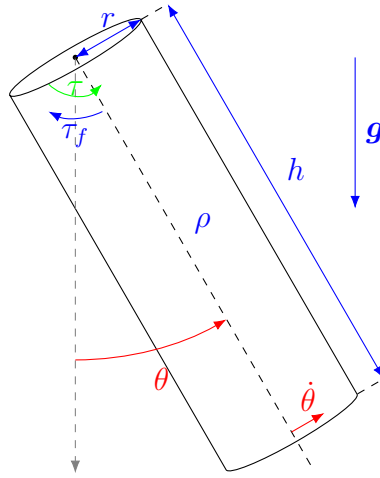


Figure 4.1: Diagram of the pendulum system. The parameters of the pendulum are in blue, the output that are fed to the controller are in red and the actuation of the controller is in green.

The value of the friction τ_f is given by

$$\tau_f = \dot{\theta}B_f \quad (4.1)$$

4.2 Sensory feedback types

The feedback sent to the bursting neuron is the heart of the stability of the neuronal system. Bad only leads to bad performances. Thus three different feedback types are proposed here. From the most simplistic feedback only relying on the angle of the pendulum to the complex spike based feedback. The goal of proposing multiple feedback is to find a middle ground between a controller complexity and its performances.

4.2.1 Angle based feedback

The direct angle feedback sends to the bursting neuron the sinus of the angle. When in the lower half of the rotational range, this value is more and more negative as the pendulum angle θ decreases and vice-versa when increasing.

Thus if the parameter of the controller are tuned to react to a value at least smaller than 1, they will act in the controller range



Figure 4.2: Diagram of the direct angle feedback.

$$I_{\text{feed}} = K_{\text{feed}} \sin(\theta) \quad (4.2)$$

with $K_{\text{feed}} > 0$ the output gain on the feedback.

4.2.2 Angle and angular velocity based feedback

This more complicated feedback aims to send a positive value to the controller only when close to the optimal control timing, which close to an angular velocity $\dot{\theta}$ close to 0. Also the feedback should only send the pulse when in the right half of the rotation plane.

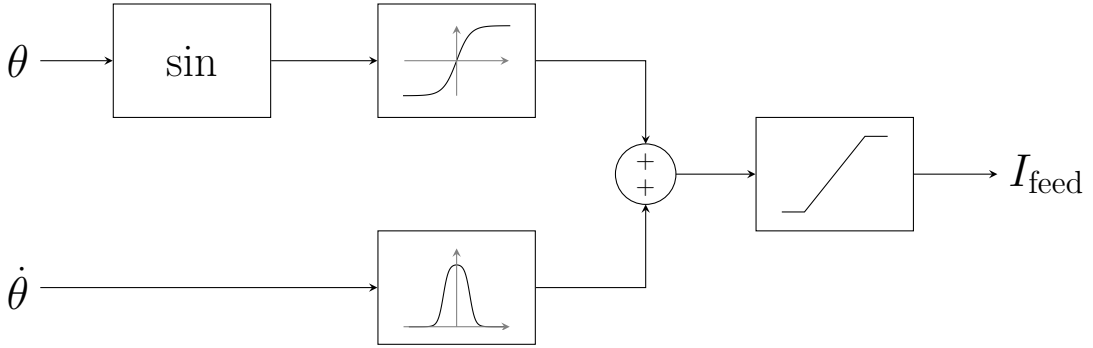


Figure 4.3: Diagram of the mixed angle and speed feedback.

$$I_\theta = \frac{\alpha_{\text{dir}} \tanh(g_\theta (\sin(\theta) - d_{\text{off}})) + 1}{2} - 1 \quad (4.3)$$

$$I_{\dot{\theta}} = \frac{\tanh(g_{\dot{\theta}} (\dot{\theta} + d_{\text{bump}})) - \tanh(g_{\dot{\theta}} (\dot{\theta} - d_{\text{bump}}))}{2} \quad (4.4)$$

$$I_{\text{feed}} = K_{\text{feed}} \min(\max(0, I_\theta + I_{\dot{\theta}}), 1) \quad (4.5)$$

with $\alpha_{\text{dir}} \in [-1; 1]$, $g_\theta, g_{\dot{\theta}}, d_{\text{bump}}, K_{\text{feed}} > 0$ and $d_{\text{off}} \in \mathbb{R}$.

α_{dir} is a parameter relative to the part of the half plane where the feedback should be active, 1 signifies an activation in the half where $\sin(\theta) > 0$ and -1 the other half. g_θ and $g_{\dot{\theta}}$ are parameters that define the sharpness of the transition of their respective tanh. d_{off} is a term that offsets I_θ to create an activation when $\theta = 0$. Since $\theta = 0$ is the resting state of the system, adding the offset avoids the system being blocked in that position. d_{bump} defines the width of the bump around $\dot{\theta} = 0$. K_{feed} is the output gain of the feedback.

4.2.3 Spike based feedback

This last feedback reuses principles from the previous feedback but seeks to reach complete neuronal control by using a spiking neuron coupled with a synapse to activate the controller. This approach has the advantage that the width of the pulse sent

to the controller remains nearly constant and not influenced by the max rotational speed.

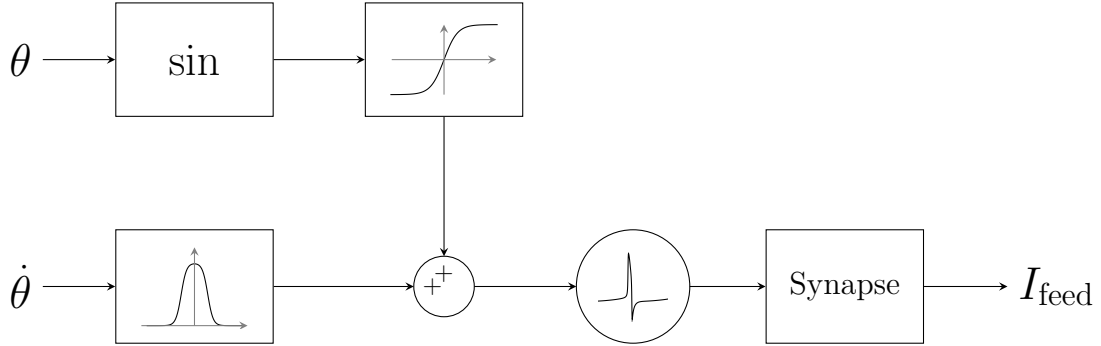


Figure 4.4: Diagram of the spike feedback.

$$I_\theta = \frac{\alpha_{\text{dir}} \tanh(g_\theta (\sin(\theta) - d_{\text{off}})) + 1}{2} - 1 \quad (4.6)$$

$$I_{\dot{\theta}} = \frac{\tanh(g_{\dot{\theta}} (\dot{\theta} + d_{\text{bump}})) - \tanh(g_{\dot{\theta}} (\dot{\theta} - d_{\text{bump}}))}{2} - 1 \quad (4.7)$$

$$V_{\text{neur}} = \text{spiking_neuron}(I_\theta + I_{\dot{\theta}}) \quad (4.8)$$

$$I_{\text{feed}} = \text{synapse}(V_{\text{neur}}) \quad (4.9)$$

with $\alpha_{\text{dir}} \in [-1; 1]$, $g_\theta, g_{\dot{\theta}}, d_{\text{bump}}, K_{\text{feed}} > 0$, $d_{\text{off}} \in \mathbb{R}$, spiking_neuron is an instance of the neuron defined in figure 3.1 and synapse is an instance of the synapse defined in figure 3.11.

α_{dir} is a parameter relative to the part of the half plane where the feedback should be active, 1 signifies an activation in the half where $\sin(\theta) > 0$ and -1 the other half. g_θ and $g_{\dot{\theta}}$ are parameters that define the sharpness of the transition of their respective tanh. d_{off} is a term that offsets I_θ to create an activation when $\theta = 0$. Since $\theta = 0$ is the resting state of the system, adding the offset avoid the system being blocked in that position. d_{bump} defines the width of the bump around $\dot{\theta} = 0$.

The parameter g_{syn} will be used as the output gain of the feedback instead of a K_{feed} parameter. Apart from that the parameters of the spiking neuron and the synapse are

g_{f-}	-2 V	g_{u+}	1 V
g_{s+}	4 V	I_{app}	0.1 A
g_{s-}	-1 V	d_{syn}	-0.5 V

while this controller should generate output similar to the simple mixed feedback, the advantage of using a neuron spike is the stability of the width of the pulse. Indeed the width of the mixed feedback is determined in part by the acceleration of the pendulum which is linked to the angle at which the speed crosses 0. The spike

of a neuron does not suffer this problem. Also, a spiking neuron has a refractory period which prevents the neuron from recreating a pulse too quickly. But, due to the inertia of the pendulum, this problem should not be encountered by the mixed feedback either.

4.3 Controller with single motor neuron

The first use of the feedbacks defined previously is to simply connect the feedback to a bursting neuron that will only be able to apply torque in a single direction. Figure 4.5 represents the proposed controller architecture. The output of the bursting neuron is passed through a saturation function that limits the output of the neuron between 0 and 1. This leads to the neuron generating torque only while bursting. The gain a the output of the saturation defines the strength of actuation.

This controller architecture is naturally imbalanced since the actuation is not symmetric and thus the damping will always lead to a lower amplitude on the side of actuation.

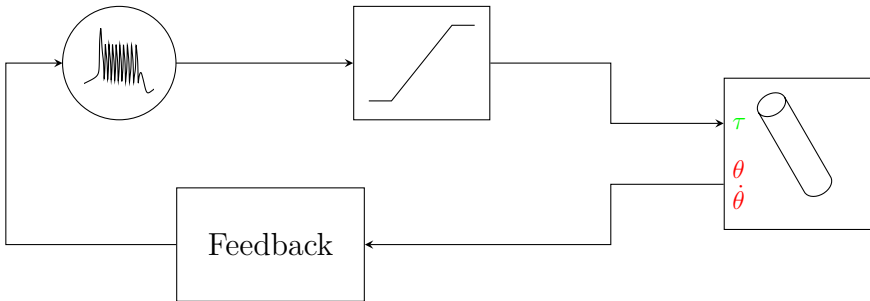


Figure 4.5: Diagram of the sensorimotor loop for the single neuron controller. The saturation block limits are 0 V to 1 V. The saturation block also contains an internal output gain τ_{\max} .

4.3.1 Performance of the sensorimotor loop

The performance of a controller can be accessed by its capabilities of generating a stable and large amplitude oscillation. To study this of the proposed controller the parameters of the bursting neuron g_{s-} , g_{u+} and I_{app} and the parameters of the strength of the feedback K_{feed} or g_{syn} are varied. Also, two different output gain $\tau_{\max} = 1$ and $\tau_{\max} = 10$ are studied to determine the appropriate force to effectively control the system.

Figures 4.6 and 4.7 shows the responses with a low output gain on the torque while figures 4.8 and 4.9. The first thing that is clear when looking at those figures is that $\tau_{\max} = 1$ is not high enough for this system to sustain large oscillation and, by extension, exercise a good control over the oscillation. Indeed the maximum range of oscillation is lower than 0.3 rad while for $\tau_{\max} = 10$ the oscillations reach

nearly 3.14 rad . So, while the maps using $\tau_{\max} = 1$ are still used, most conclusion are drawn from the maps using $\tau_{\max} = 10$.

Figures 4.6a, 4.7a, 4.8a and 4.9a shows that most of the time the mixed and spiking feedback are able to generate oscillation with lower I_{app} . Now looking at Figures 4.8b and 4.9b shows that the mixed and spiking feedback are able to reach the oscillations with the greatest amplitudes.

Now looking at $I_{\text{app}} = -1 \text{ A}$ and especially $I_{\text{app}} = 0 \text{ A}$, the maps of the controller with feedback become closer to the map of the controller using no feedback. This indicates that those higher I_{app} are not as relevant since they lead to a behavior close to no feedback and this can only lead to poor control. The range of oscillation maps confirm this since they show that higher I_{app} lead to far lower oscillation amplitude. This shows the poorness of the control, since a efficient control should be able to generate high amplitude oscillations.

In figure 4.9b the map of the mixed or the spiking feedback when $I_{\text{app}} = -2 \text{ A}$ seems to validate figures 3.7 and 3.8 as lowering g_{s-} is well correlated with the amplitude of the oscillations. This shows the link between the value of g_{s-} and the power contained in a burst.

Now comparing the different feedback it seems that the sinusoidal feedback has a behavior different from the mixed and spiked feedback. Meanwhile, the mixed and the spiked feedback have very similar behaviors. This can be explained since the mixed feedback is a spike-like behavior near $\dot{\theta} = 0$ and the spike feedback neuron is excited when near to $\dot{\theta} = 0$. Thus both feedback generate a spike when the angular velocity is low. But, it must be noted that in figure 4.7 the spiking feedback generates relatively more oscillation than the mixed feedback model.

The analysis of the maps seems to point toward low I_{app} , high τ_{\max} , high strength of feedback and mixed or spiking feedback as the best controller.

But, the analysis gave rise to the highlight of some zones of interest. Figure 4.10 shows the oscillation generated in three different interesting zone.

The first four rows of traces show the behavior of all feedback types at the specific point seen in figure 4.9 where the uncoupled bursting neuron is able to generate large oscillation. The idea is to investigate why the system have receiving no information about the state of the pendulum is able to generate "good" oscillation and what adding feedback can do in the same situation. Looking at the traces of the angle θ for the no feedback case, it seems that the frequency of bursting aligns by chance with the frequency of pendulum. The match is not perfect since the amplitude of oscillation varies a bit but still remains in a small range. Now looking at the effect of the feedbacks when using the same parameter for bursting and choosing the highest sensory feedback strength, the oscillation pattern does not change. Some phase is introduced between feedback types since the bursting patterns are not in sync but the shape of a burst and the inter-burst frequency is nearly the same in all cases. This highlights a very important behavior, if the neuron has a high base excitatory current, which is the case here since figure 3.3 indicates that bursting with these parameters starts a bit above $I_{\text{app}} = -2 \text{ A}$, then the feedback becomes less effective and thus the connection between the neuron and the mechanical system

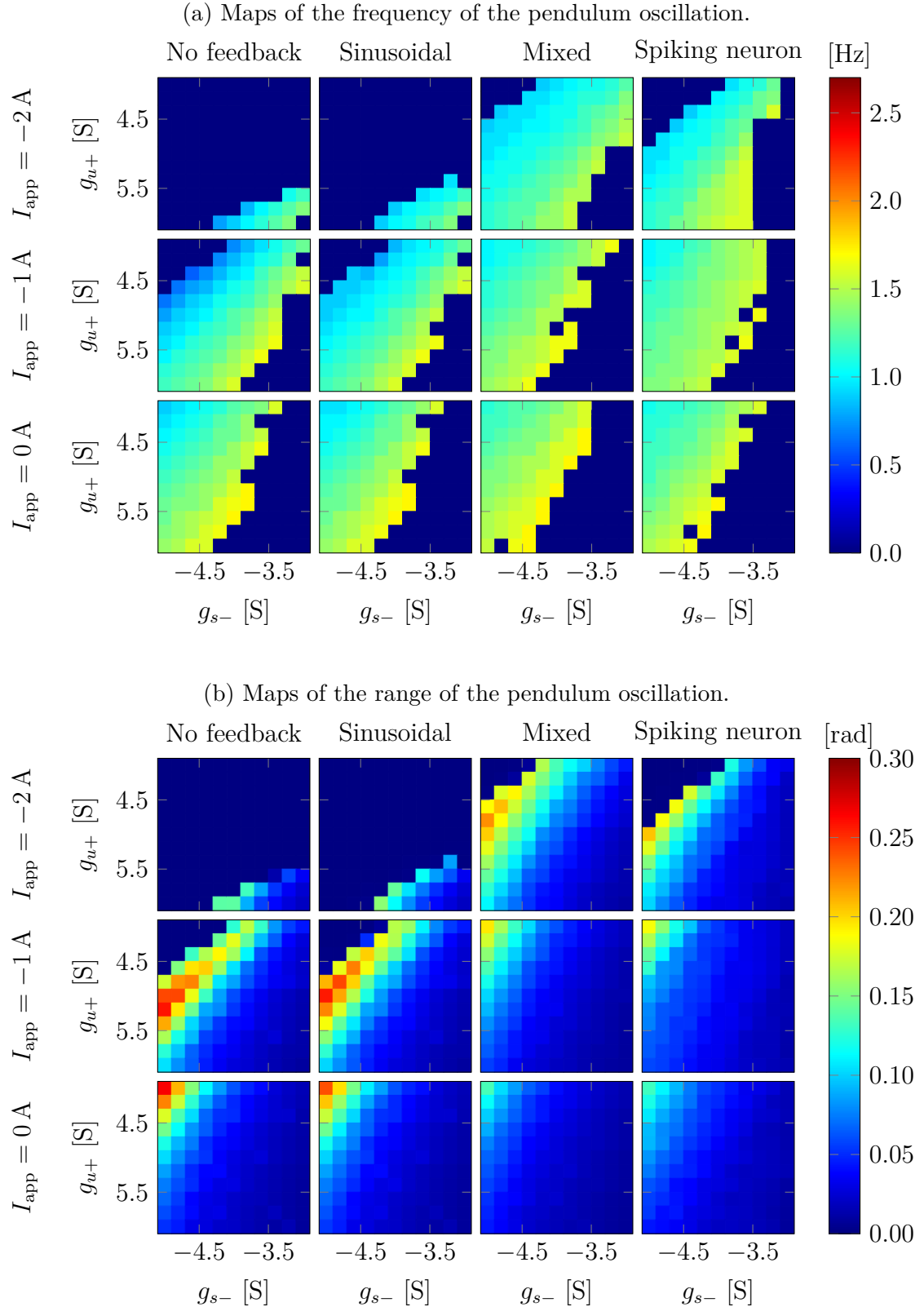


Figure 4.6: Diagram of system behavior with $\tau_{\max} = 1 \text{ N m V}^{-1}$ and $K_{\text{feed}} = 1$ or $g_{\text{syn}} = 1 \text{ S}$.

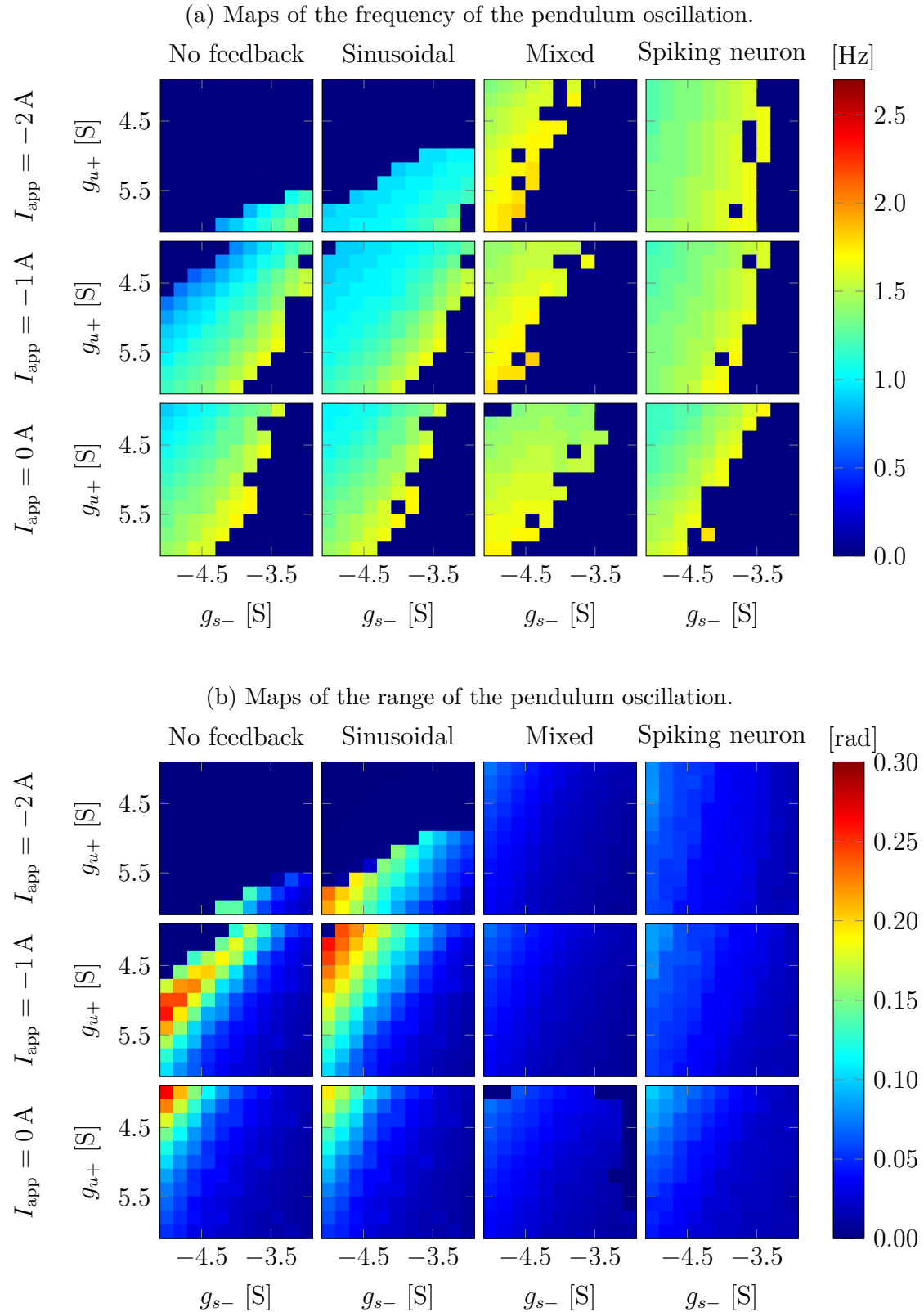


Figure 4.7: Diagram of system behavior with $\tau_{\max} = 1\text{ N m V}^{-1}$ and $K_{\text{feed}} = 5$ or $g_{\text{syn}} = 3\text{ S}$.

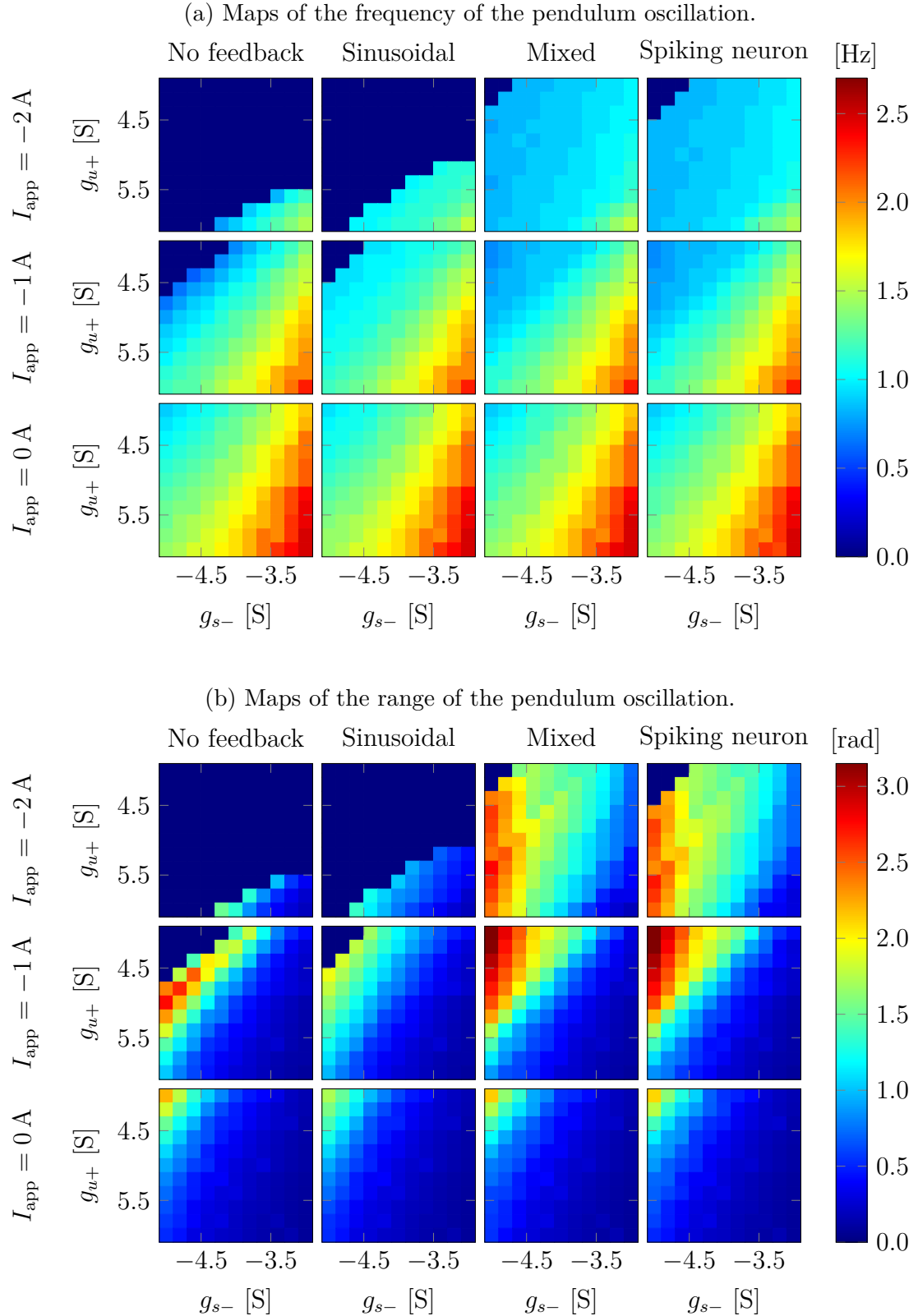


Figure 4.8: Diagram of system behavior with $\tau_{\max} = 10 \text{ N m V}^{-1}$ and $K_{\text{feed}} = 1$ or $g_{\text{syn}} = 1 \text{ S}$.

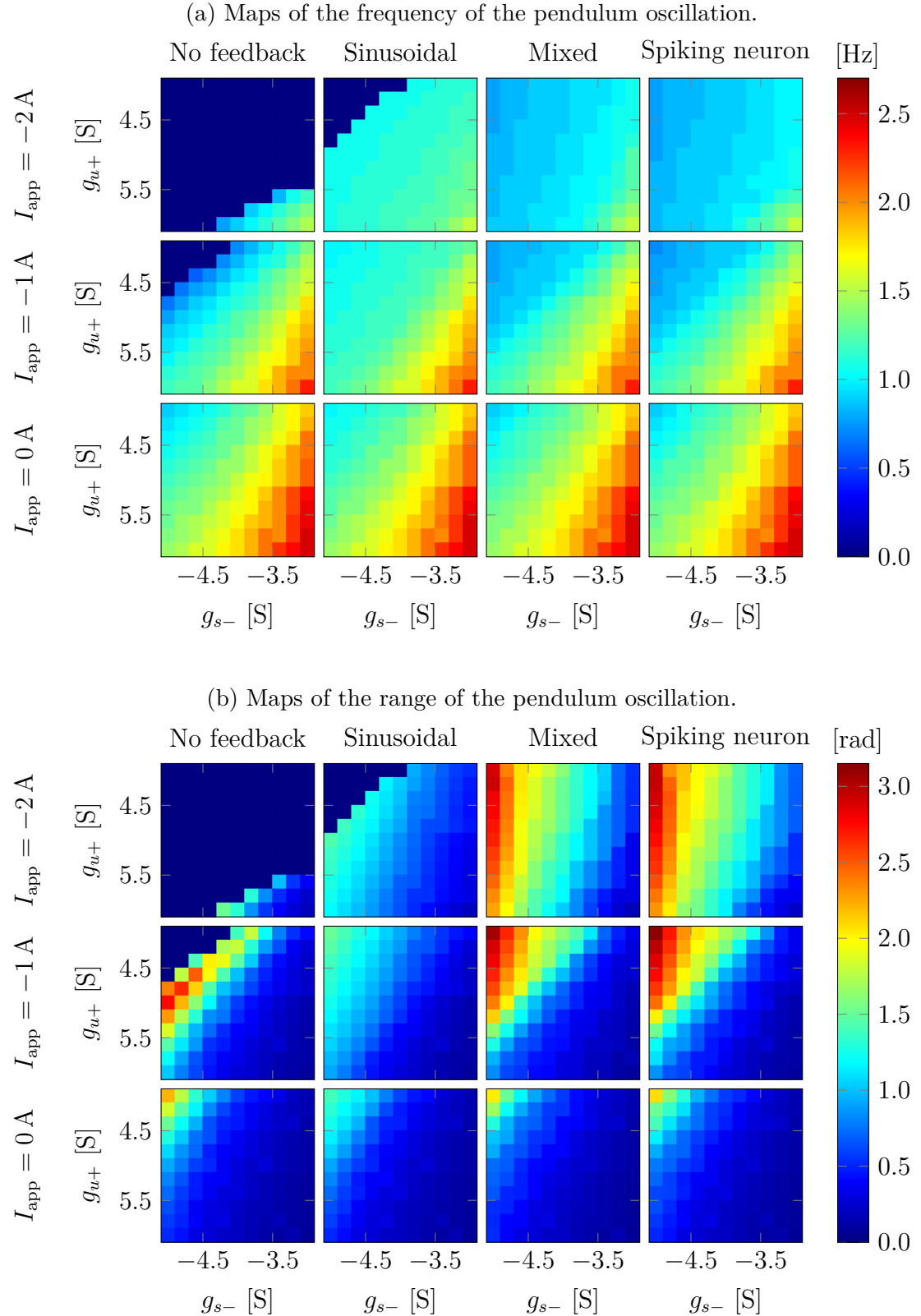


Figure 4.9: Diagram of system behavior with $\tau_{\max} = 10 \text{ N m V}^{-1}$ and $K_{\text{feed}} = 5$ or $g_{\text{syn}} = 3 \text{ S}$.

is diminished. This is the opposite of the desired behavior.

Next, the fifth and sixth rows in figure 4.10 show a more desirable behavior. There, the mixed and neuron feedback are shown with a better set of parameter seen in figure 4.9. Here, the lower base current allows the feedback to dominate the activation of the neuron. This result in a strong connection between the neuron and the mechanical system. The traces of the oscillation confirm that since they have greater amplitude than for parameter discussed before and are extremely regular. The regularity of those oscillation really demonstrate the link between the neuron and the pendulum since a perfect match between the inter-burst frequency and the oscillation frequency is only possible if the bursting is mostly started by the feedback.

Lastly, for most of the analysis the mixed and the neuronal feedback were grouped together and shown to have identical performances. But they are not the same and in specific cases they display different behaviors. The seventh and eighth rows in figure 4.10 display this difference. The parameter are taken from figure 4.6 where the low current behavior seemed quite different. And indeed the traces confirm they are. The mixed feedback seems to be stuck in a behavior similar to the first row but with far smaller oscillation due to the lower gain on the torque. This appears clearly with the variation of the amplitude of each oscillation and the seemingly constant bursting of the neuron. On the other hand the neuron feedback is able to generate far larger and more regular oscillations despite being subject to the same parameters. This difference can be explained easily when thinking about the nature of the feedback. This boils down to the fact that the mixed feedback is continuous while the neuron feedback is by nature event based. This may seems a bit strange since the mixed feedback when declared in section 4.2.2 was described as generating pulses. But, looking back at the equations governing the feedback reveals that it only holds true if the angular velocity is high and then equation (4.4) is zero except at the peak of the oscillation where the speed is close to zero. In the case where the torque is low the system may become stuck in a pattern of very small oscillation that, due the limited torque and range, do not have the velocity to get out the bump. Thus the mixed feedback can be abstracted as equation (4.4) plus one, which is a feedback only based on the position. In the neuronal cases things are different. Even if the input to the spiking neuron is similar to the mixed feedback, passing this into a neuron transform this continuous feedback into event. If the neuronal feedback was put in the exact same position as the mixed feedback it would spike at a relatively low frequency leading to a more stable activation allowing it to exit the position and generate larger oscillations.

4.3.2 Robustness of the sensorimotor loop

In a real controller it is nearly impossible to achieve the exact theoretical parameters. It is therefore important to analyze the behavior of the controller when the parameters deviate from the ideal values. In the previous section good parameters were found to be around $I_{app} = -2 \text{ A}$, $g_{s-} = -5 \text{ S}$ and $g_{u+} = 5 \text{ S}$.

The classical way of doing such an analysis is simply to use Monte-Carlo by

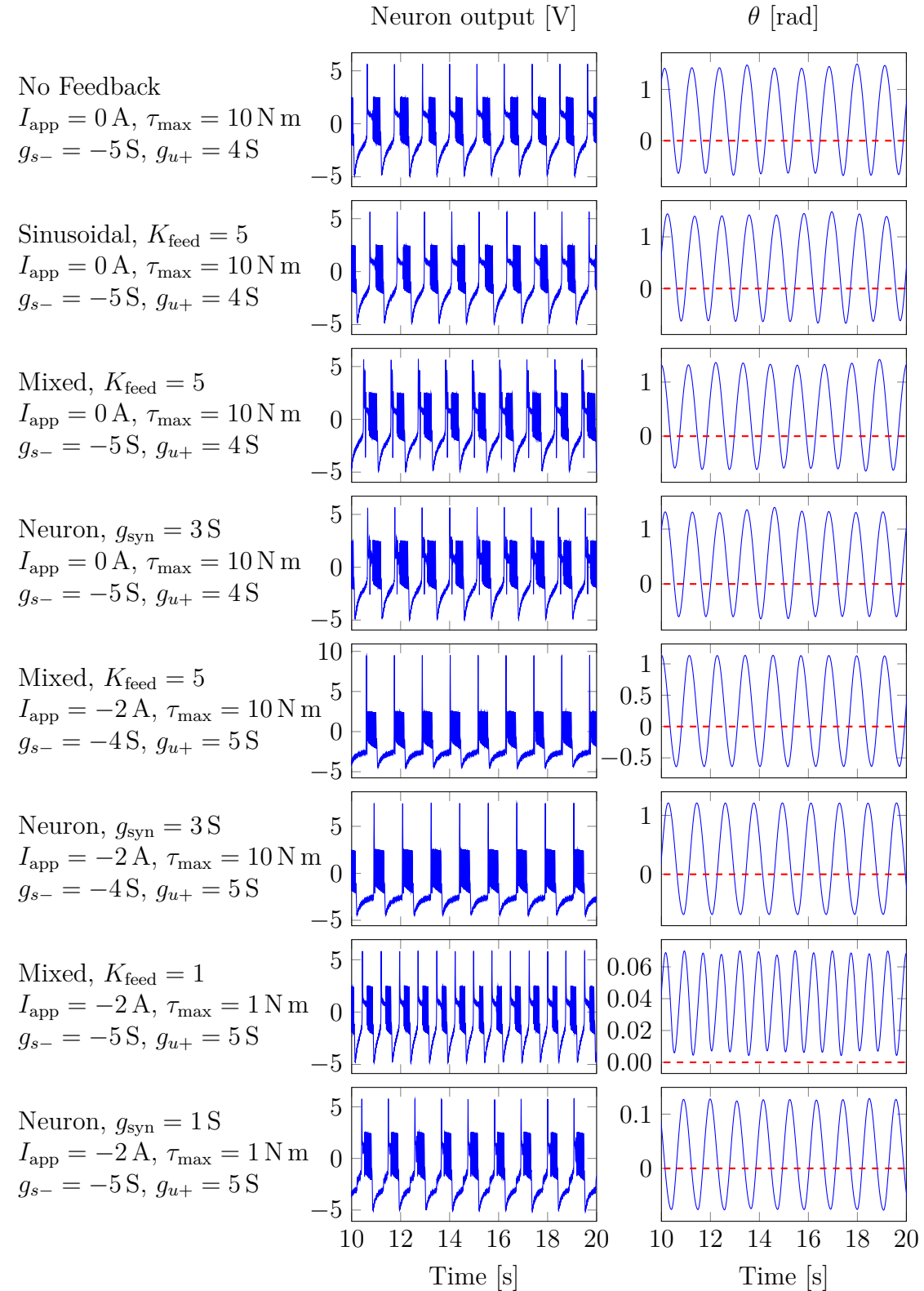


Figure 4.10: Temporal behavior of the single bursting neuron system under different parameters and with different feedback.

sampling the parameters from a certain distribution centered around the ideal values and plot the distributions of relevant output value to visualize the influence of these changing parameters on the control. Before doing this, the robustness can already be assessed in figures 4.6 to 4.9 by looking at the change in values around the chosen parameters. Since $\tau_{\max} = 10 \text{ N m V}^{-1}$ and $K_{\text{feed}} = 5$ or $g_{\text{syn}} = 3 \text{ S}$ gave the best controller results those parameters will be used and thus only figure 4.9 is relevant. The maps of frequency and oscillation in that figure show us that there is a relative stability around the good parameters at least in the g_{s-} and g_{u+} dimensions. Here, relative stability means that the gradient of in the frequency map and the amplitude map is relatively low in amplitude and there are no big discontinuities.

To have a point of comparison and further prove the point of the previous chapter, the fragile bursting displayed in figures 3.5 and 3.6 is chosen to compare the good parameters with a poor control. To represent this behavior the fragile bursting has the parameters $I_{\text{app}} = 0 \text{ A}$, $g_{s-} = -0.1 \text{ S}$ and $g_{u+} = 4 \text{ S}$. $I_{\text{app}} = 0 \text{ A}$ was chosen to put the fragile neuron in a similar point to the robust neuron meaning being before the natural bursting.

With all that, figure 4.11 displays the histograms resulting from the Monte-Carlo simulations on the robust and fragile neuron coupled with all feedbacks previously defined.

The first observation that can be made by looking at the distribution of in figure 4.11a is that the robust neuron is very precise and is able to keep the oscillation at the same frequency except the mixed feedback which displays two very close frequencies. On the other hand the fragile neuron is much worse with the dominant frequency being spread over a large range of frequencies. Especially in the case with no feedback and with sinusoidal feedback. Yet, the mixed feedback is again different from the others with a behavior very similar to the robust neuron except at a slightly higher frequency.

Looking at the the amplitude of oscillation in figure 4.11b gives a clearer picture of what is happening. The amplitudes of oscillations of the robust neuron are far larger than the oscillations of the fragile neuron. In fact, apart in the case of the mixed feedback, the range of oscillation of the fragile neuron is nearly zero, proving that it is inn effective at generating oscillation. It is also interesting to note that the range of the robust neuron with no feedback is perfectly zero, which is normal since the bursting neuron is inactivated. But, it is not the case for the fragile neuron which shows again that, as presented in figure 3.6, the fragile neuron is very sensible to noise.

Figure 4.12 is a zoom on the behavior of the robust neuron. This figure highlights what was already supposed previously. The principal frequencies of oscillation are shown to be very stable. The sinusoidal and spiking neuron feedback lead to a single frequency while the mixed feedback lead to two separate frequencies, there is no distribution on the frequency range. Now looking at the range of oscillation, while all feedbacks span a similar range of around 0.1 rad the sinusoidal feedback seems to spread more than the other two feedback. Those other feedbacks seemed to have a large narrow peak and then a small wider peak with a space of no oscillation

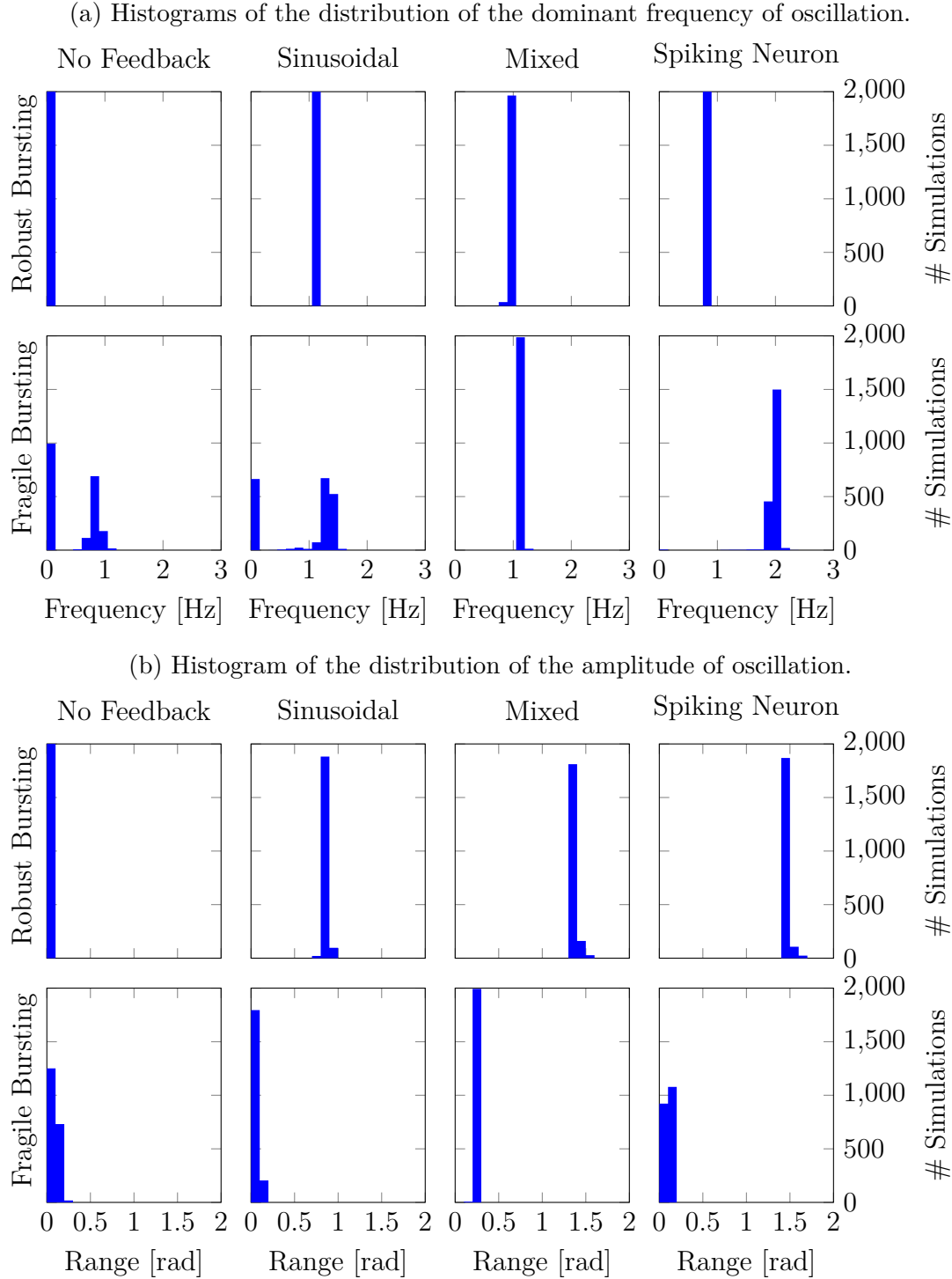
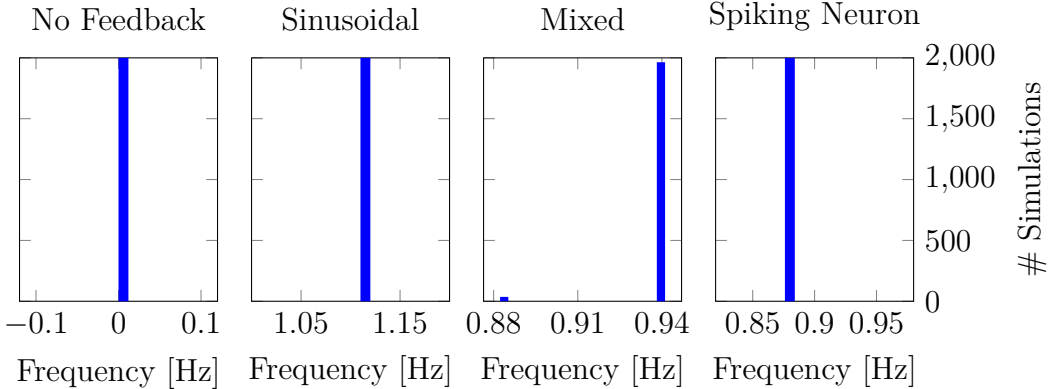


Figure 4.11: Comparison of the robustness of all feedbacks on the single neuron controller using Monte Carlo analysis. The parameters of the robust bursting were sampled from $I_{app} \sim \mathcal{N}(-2, 0.05^2)$ A, $g_{s-} \sim \mathcal{N}(-4, 0.03^2)$ S and $g_{u+} \sim \mathcal{N}(5, 0.05^2)$ S. The parameters of the fragile bursting were sampled from $I_{app} \sim \mathcal{N}(0, 0.05^2)$ A, $g_{s-} \sim \mathcal{N}(-0.1, 0.03^2)$ S and $g_{u+} \sim \mathcal{N}(4, 0.05^2)$ S. Both bursting used $g_{f-} = -2$ S, $g_{s+} = 6$ S, $\tau_{max} = 10$ N m V $^{-1}$ and $K_{feed} = 5$ or $g_{syn} = 3$ S.

between. This shows a more precise control of the mixed and spiking feedback. Yet, this second smaller is strange given the single frequency found. This behavior could be explained in the case of the mixed feedback with the two separate frequencies but the amount of simulation in the second peak of higher amplitude is higher than the number of simulation in the smallest frequency so this cannot explain the entire peak. This is due to the dominant frequency being the frequency with the highest power thus it can be quite stable even if the oscillation changes a bit.

(a) Histograms of the distribution of the dominant frequency of oscillation.



(b) Histogram of the distribution of the amplitude of oscillation.

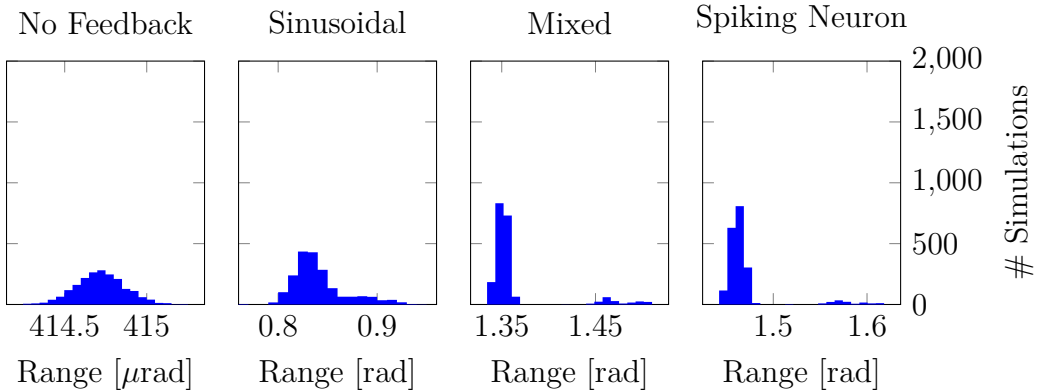


Figure 4.12: Comparison of the robustness of all feedbacks on the single neuron controller using Monte Carlo analysis. The parameters of the bursting were sampled from $I_{app} \sim \mathcal{N}(-2, 0.05^2)$ A, $g_{s-} \sim \mathcal{N}(-4, 0.03^2)$ S and $g_{u+} \sim \mathcal{N}(5, 0.05^2)$ S. The bursting also used $g_{f-} = -2$ S, $g_{s+} = 6$ S, $\tau_{max} = 10$ N m V⁻¹ and $K_{feed} = 5$ or $g_{syn} = 3$ S. Zoom on only the behavior of the robust neuron.

4.4 Two neuron "push-pull" controller

The next step in the controller design is to make it symmetrical by adding a new bursting neuron and another feedback block for it. Also to enforce the alternating activation of the bursting neurons they are mutually connected by inhibitory

synapses. This turns the two neurons into a half-center oscillator. This is done two avoid a simultaneous activation of the neurons since it would be suboptimal to push in both rotational directions at the same time.

Obviously, the feedback to the new bursting neuron will be tailored to mirror the feedback to the first in order to activate in the other half of the rotation plane.

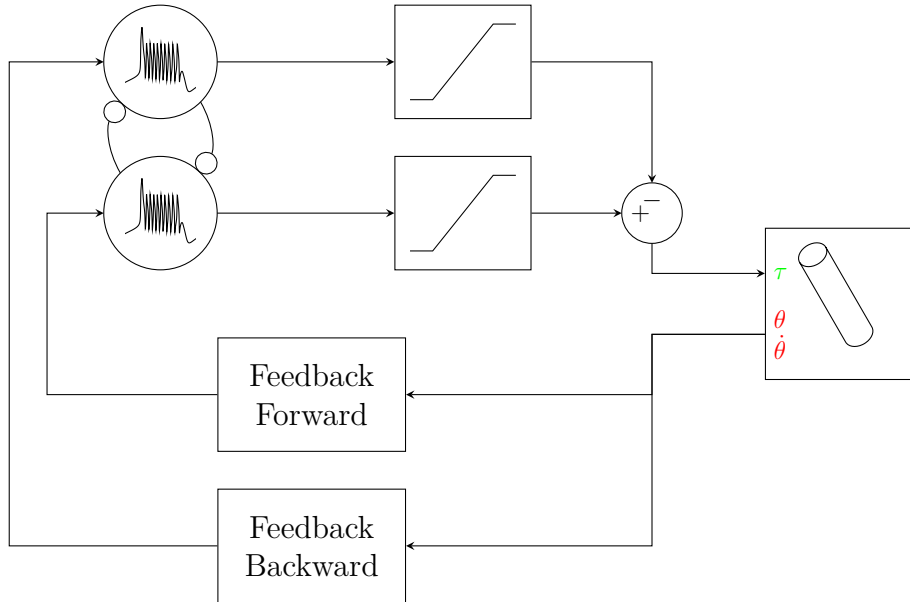


Figure 4.13: Diagram of the sensorimotor loop for the two neurons push-pull controller. The saturation block limits are 0 V to 1 V. The adding block also contains an internal output gain τ_{\max} . The bursting neurons are connected by inhibitory synapses.

The synapses have the same parameters since the system should be symmetrical. The parameters are $d_{\text{syn}} = 0.0 \text{ V}$ and $g_{\text{syn}} = -1 \text{ S}$.

4.4.1 Performance of the sensorimotor loop

Like the test for the single neuron controller, the performances of this new controller can be accessed by its capabilities of generating a stable and large amplitude oscillation. In the same manner, to study this of the proposed controller the parameters of the bursting neuron g_{s-} , g_{u+} and I_{app} and the parameters of the strength of the feedback K_{feed} or g_{syn} are varied. Also, two different output gain $\tau_{\max} = 1$ and $\tau_{\max} = 10$ are studied to determine the appropriate force to effectively control the system.

Figures 4.14 to 4.17 display the behavior of the double neuron system in the same manner as figures 4.6 to 4.9 that were used for the single neuron controller.

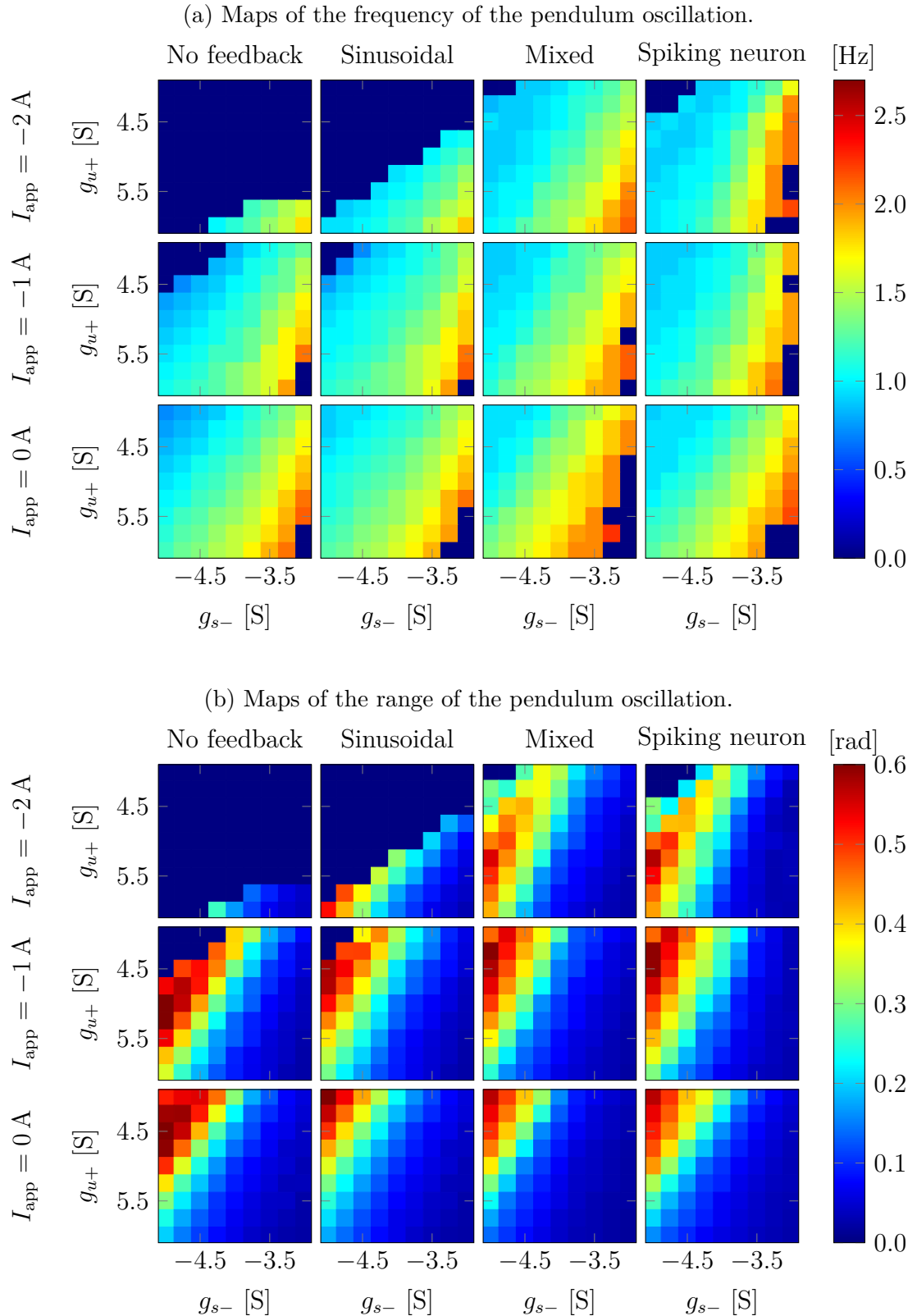
The first thing that is flagrant in this situation is that the sinusoidal feedback always leads to far lower amplitude of oscillation compared to the mixed of spiking neuron feedback. Except for $\tau_{\max} = 1$ and $K_{\text{feed}} = 5$ where figure 4.15 shows that

the mixed feedback seems to fail. Those lower oscillations are mostly due to the feedback being directly linked to angle leading to an activation that is too early and does not manage to reach large amplitudes. Indeed in figures 4.14 and 4.15 while still visible, the amplitude displayed is far better since the lower maximum torque restricts the possible oscillation range.

Now, analyzing the amplitude part of the results clearly shows the gain of adding another control neuron allows far greater amplitude to be reached. Figure 4.9 showed a maximum amplitude around π while figure 4.15 reaches 2π which is a full circle, that is impressive.

What is also interesting is that the CPG connection allows the no feedback system to still generate sizable oscillation. This is linked to the natural oscillatory nature of the connection (see figure 3.12). Those oscillation lacking sensory feedback are naturally not attuned to the frequency of the pendulum and should generate very chaotic movement. Yet, this displays quite well the usefulness of the CPG, it intrinsically capture the necessary order of actuation of this system.

4.4.2 Robustness of the sensorimotor loop


 Figure 4.14: Diagram of system behavior with $\tau_{\max} = 1$ and $K_{\text{feed}} = 1$ or $g_{\text{syn}} = 1$.

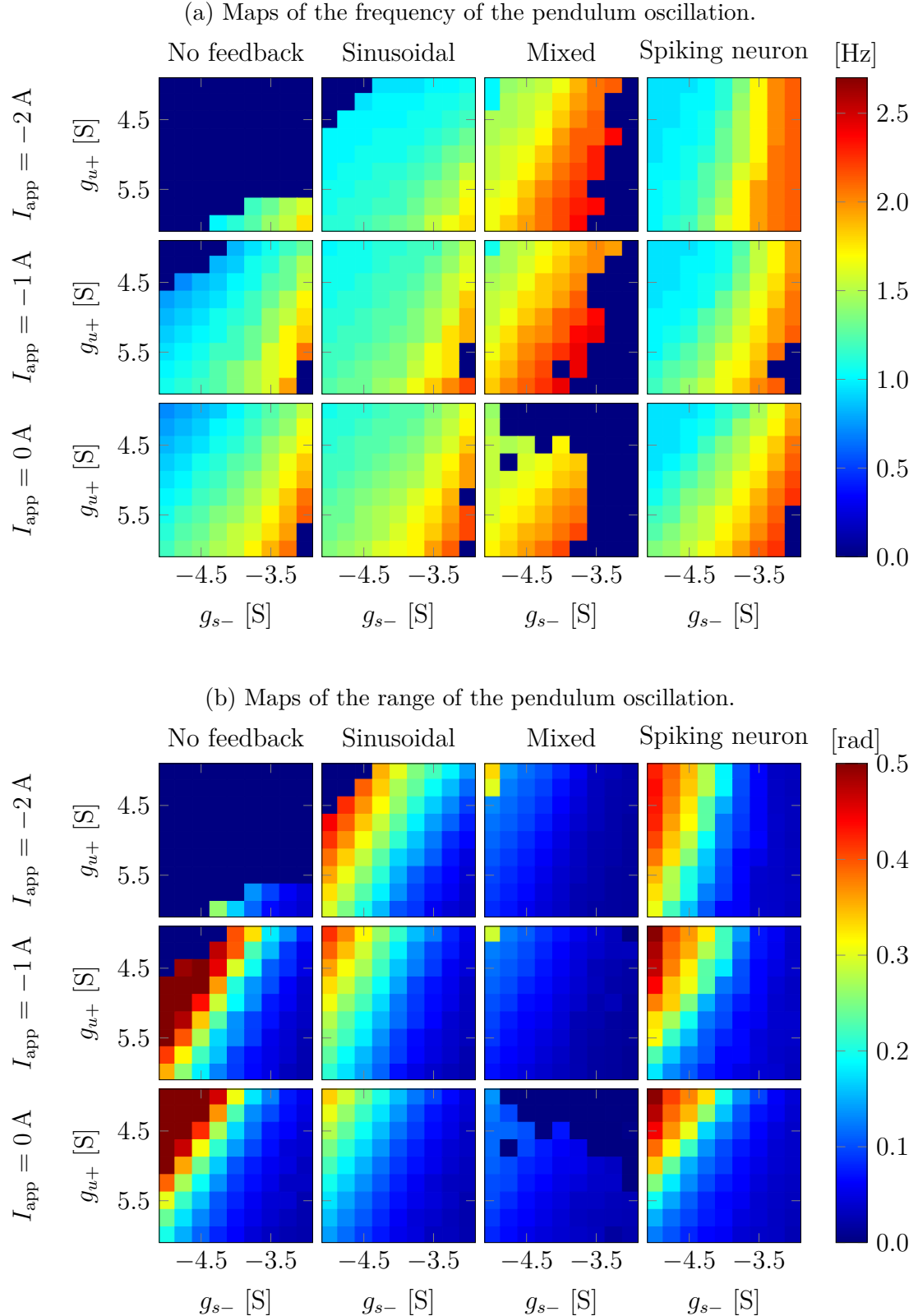
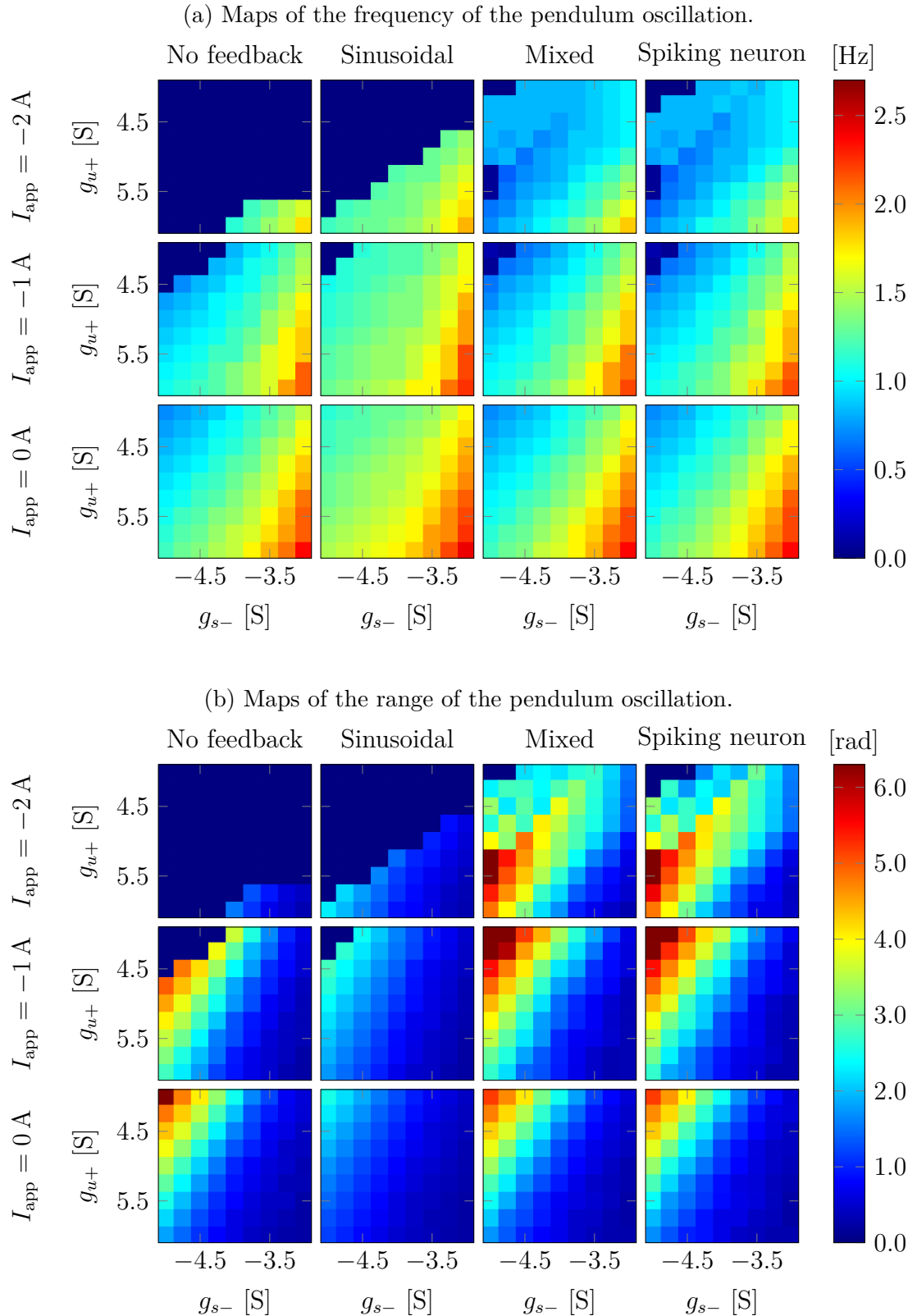
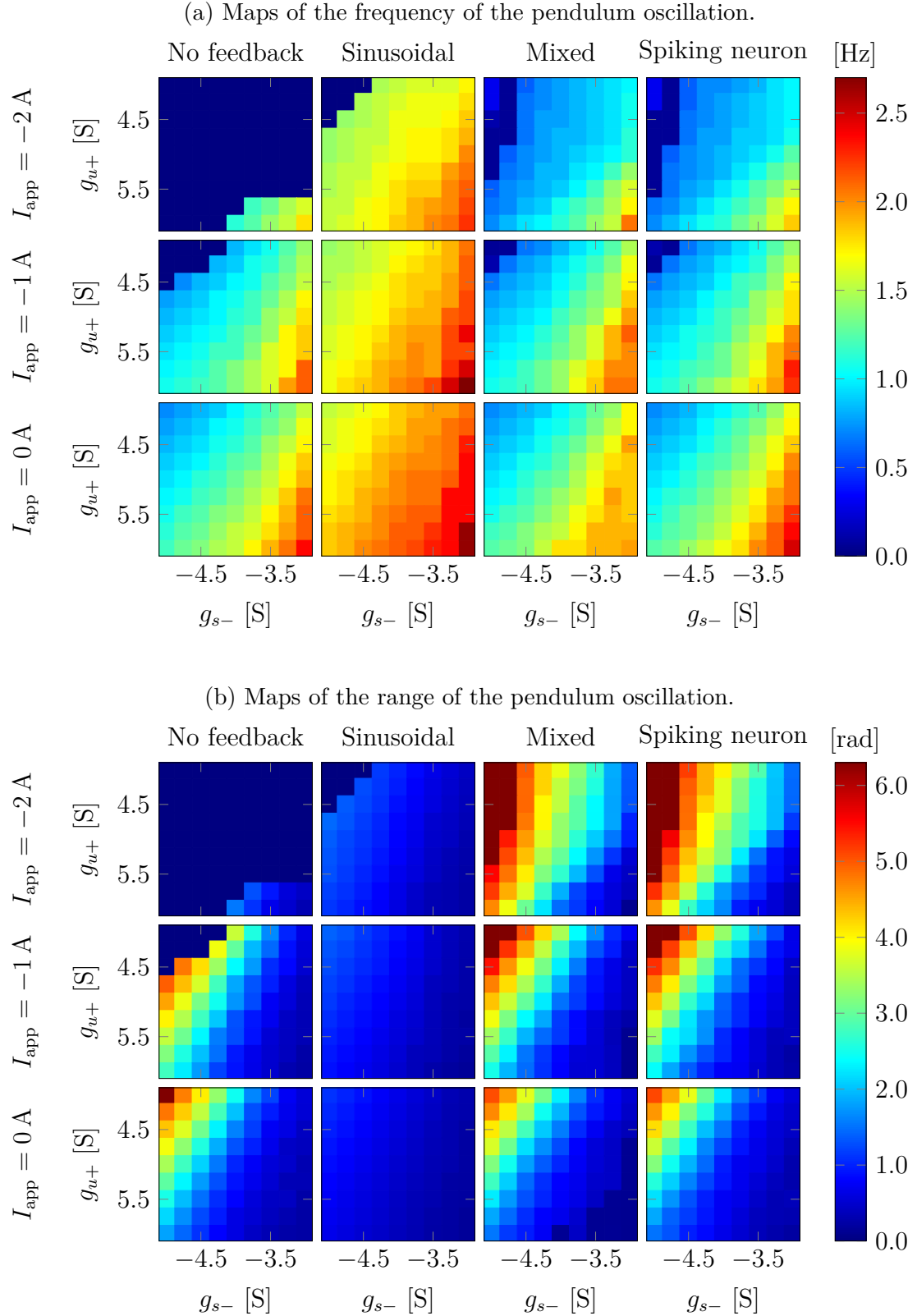


Figure 4.15: Diagram of system behavior with $\tau_{max} = 1$ and $K_{feed} = 5$ or $g_{syn} = 3$.

Figure 4.16: Diagram of system behavior with $\tau_{\max} = 10$ and $K_{\text{feed}} = 1$ or $g_{\text{syn}} = 1$.

Figure 4.17: Diagram of system behavior with $\tau_{\max} = 10$ and $K_{\text{feed}} = 5$ or $g_{\text{syn}} = 3$.

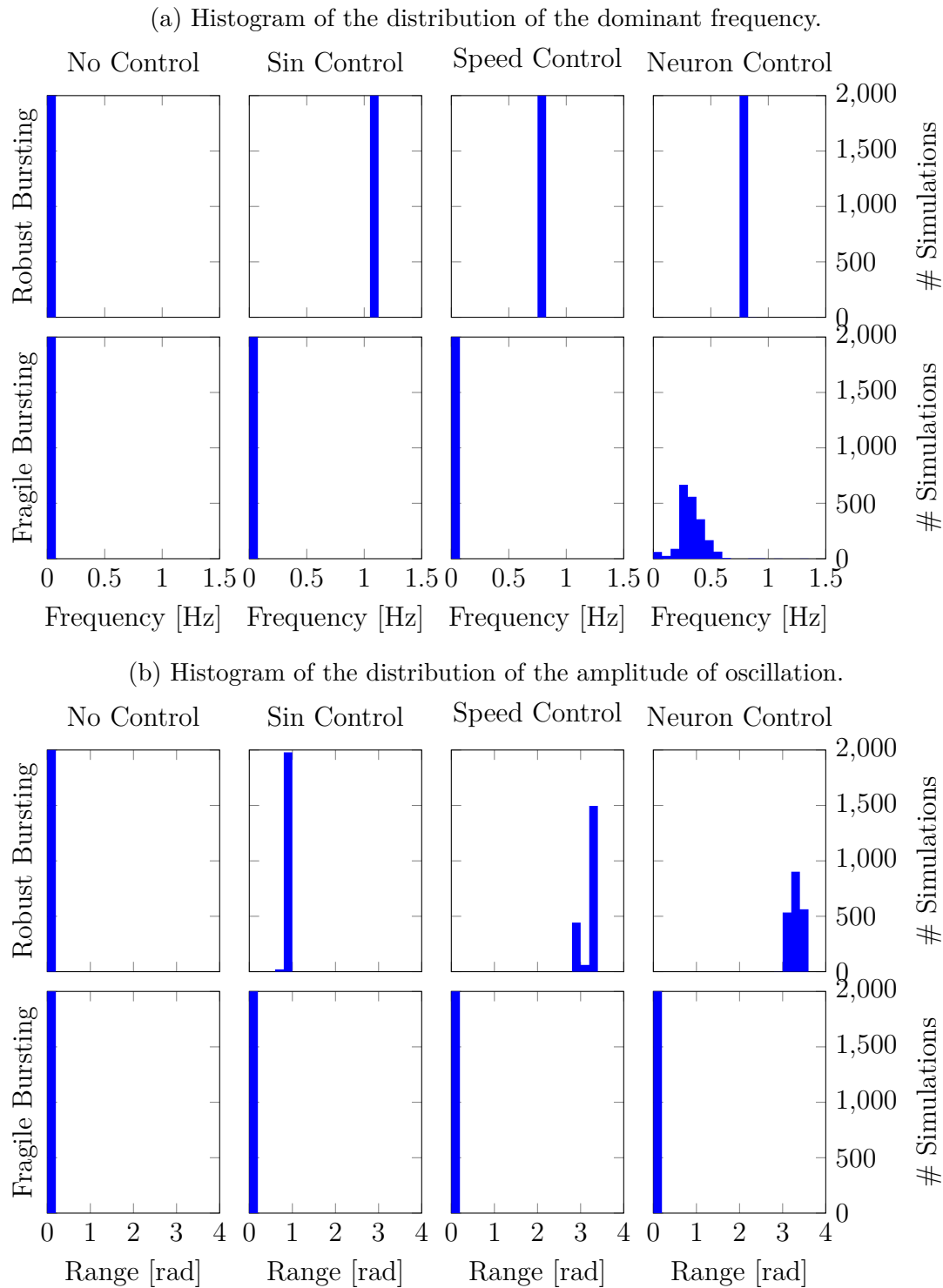


Figure 4.18: Comparison of all controllers using Monte Carlo analysis on the controller parameters.

Chapter 5

Neuromodulation for adaptive amplitude control

The previous chapter established a strongly connected sensorimotor system. But, the control of the oscillation was nearly impossible and required change in the model parameter. This chapter introduce a neuromodulation model that is able to automatically modify the neuron parameters to reach a target amplitude.

5.1 Design of the controller

The neuromodulation is added to the two system defined in chapter 4. The parameter neuromodulated is g_{s-} since section 3.3.1 established that this was a good parameter to control the power transmitted by a burst. Figure 5.1 displays the diagram of the model. This diagram add two new spiking neuron whose output are passed through a saturation to only have a non-zero output when spiking. The output of these neurons are merged and fed through an integrator. The output of this integrator is then fed to a low-pass filter. The output of this filter is the parameter g_{s-} .

The idea of this architecture is to have the spiking increase or decrease the value of g_{s-} by steps and the low-pass filter is only there to smooth the value of the parameter and avoid weird neuronal behaviors due to steps in the parameters.

The feedback fed to those spiking neuron is vastly different from the feedback to the bursting neurons. Figure 5.2 displays this different architecture. It can be understood as a check of the amplitude at the peak of the oscillation. One neuron will spike if the amplitude is too low and the other will spike if it is too high. The parameter *IDK* defines a zone near the desired amplitude that is deemed acceptable.

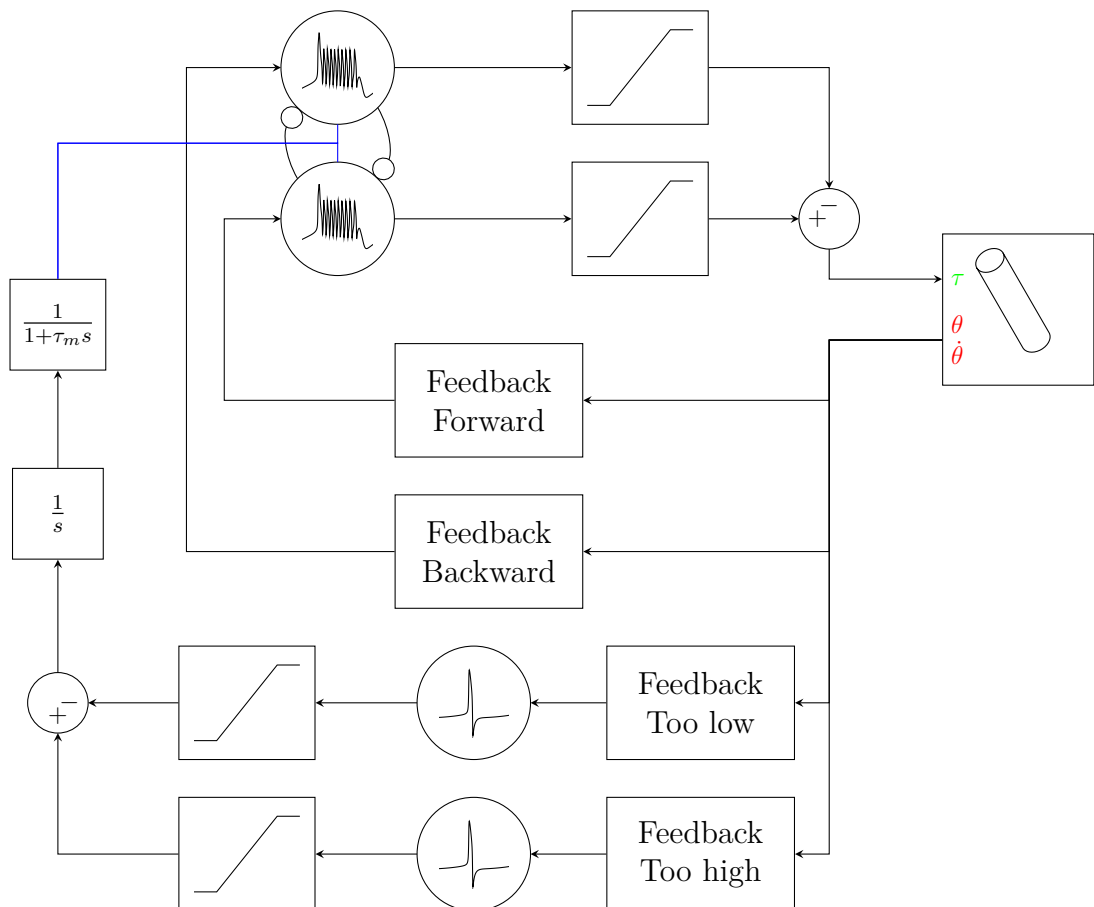


Figure 5.1: Diagram of the control loop of the controller with neuromodulation. The adding blocks also contain internal output gains. The bursting neurons are connected by inhibitory synapses. Blue lines represent parameters and not input/output values.

Figure 5.2: Diagram of the neuromodulation feedback.

$$I_\theta = \sigma(g_\theta(\cos(\theta_{\text{ref}}) - \cos(\theta))) \quad (5.1)$$

$$I_{\dot{\theta}} = \frac{\tanh(g_{\dot{\theta}}(\dot{\theta} + d_{\text{bump}})) - \tanh(g_{\dot{\theta}}(\dot{\theta} - d_{\text{bump}}))}{2} - 1 \quad (5.2)$$

$$I_{\text{feed}} = K_{\text{feed}} \min(\max(0, I_\theta + I_{\dot{\theta}}), 1) \quad (5.3)$$

5.2 Controller performance

5.2.1 Static

5.2.2 Dynamic

5.3 Robustness analysis

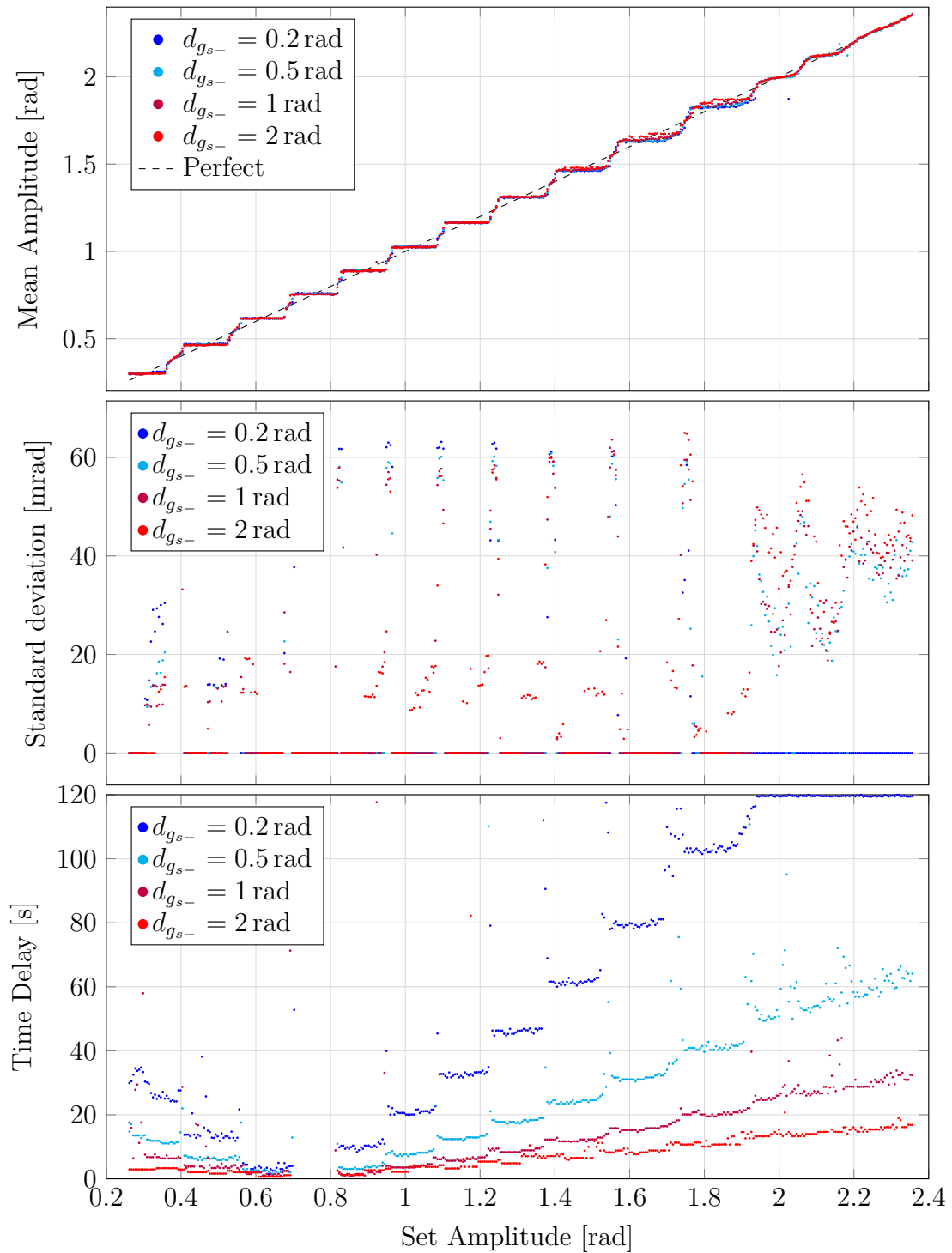


Figure 5.3: Desired angle vs realized angle.

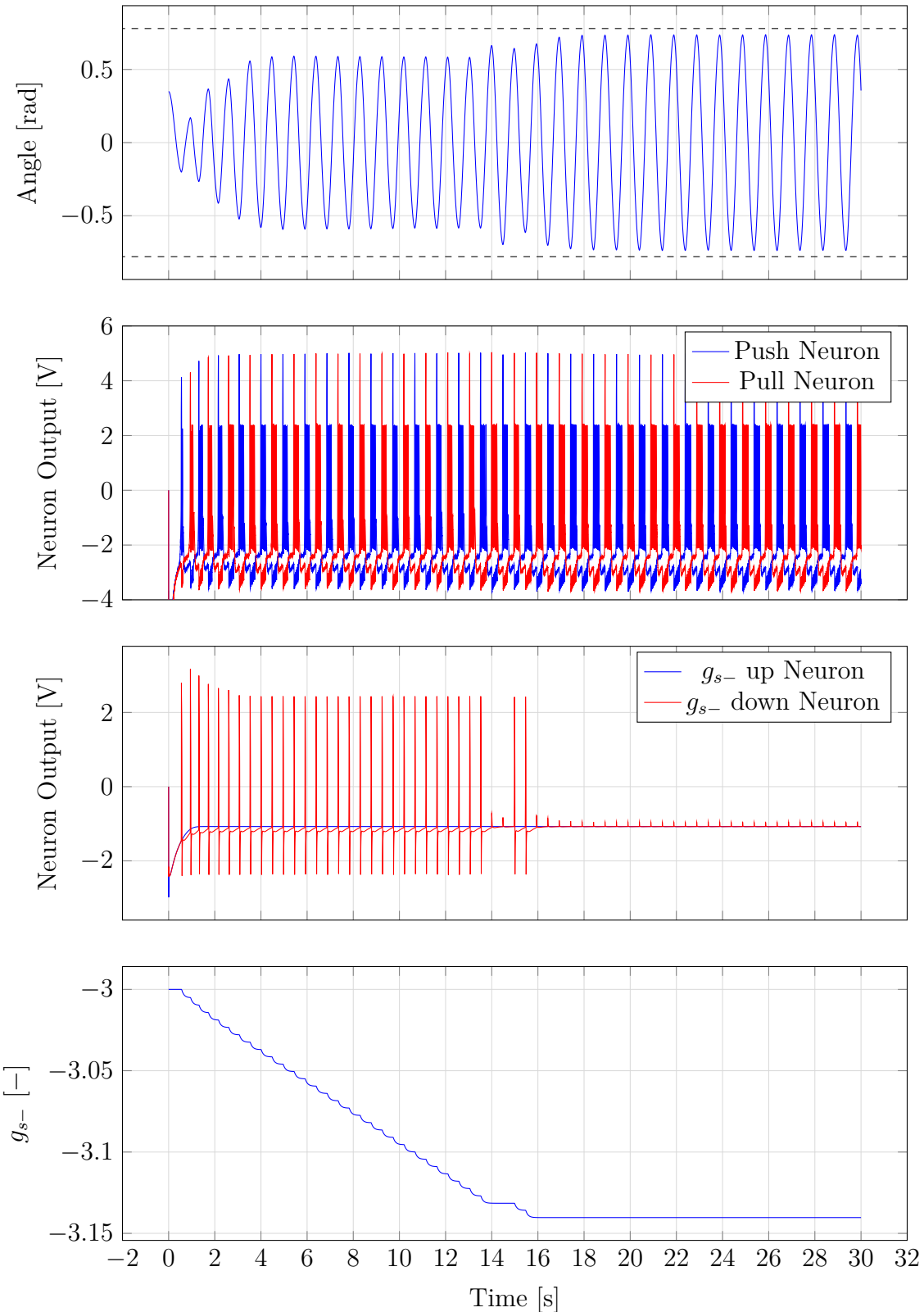


Figure 5.4: Oscillation of the pendulum in a neuromodulated case where the initial oscillation is smaller than desired.

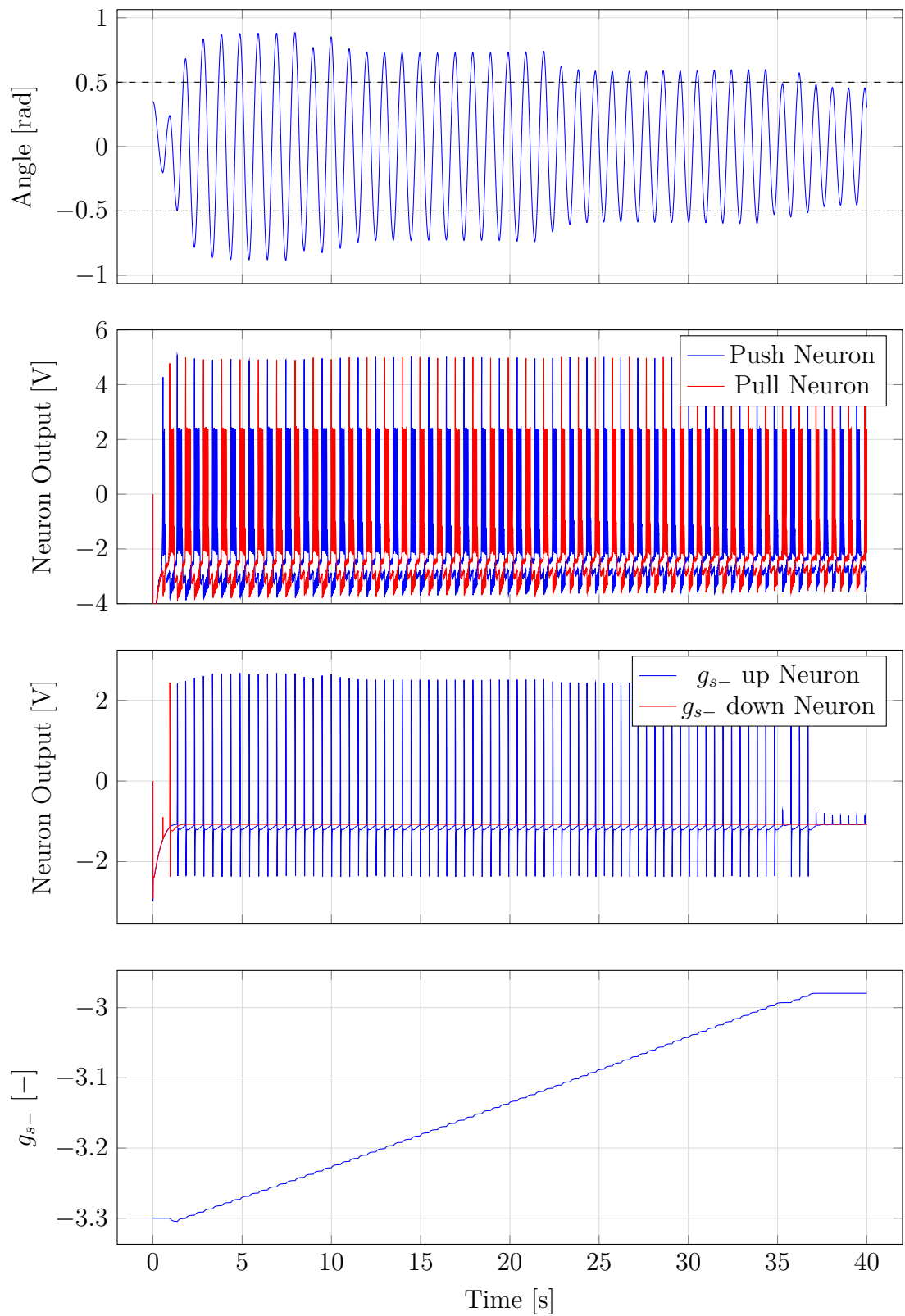


Figure 5.5: Oscillation of the pendulum in a neuromodulated case where the initial oscillation is higher than desired.

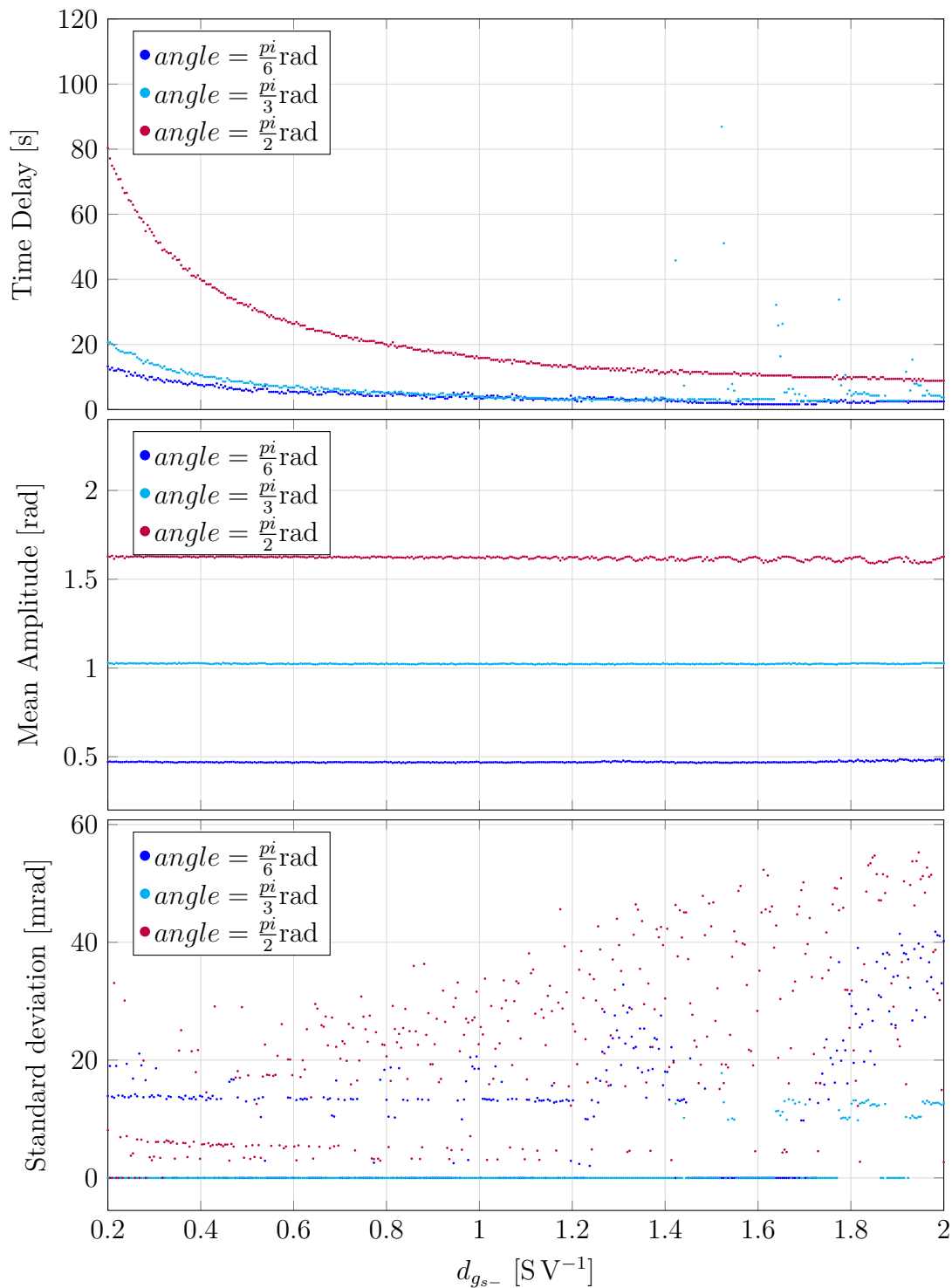


Figure 5.6: Desired angle vs realized angle.

Chapter 6

Conclusion

This thesis started from a simple neuronal model and coupled it with a mechanical system to reach stable oscillation. This goal led to the definition of multiple sensory feedback to couple the mechanical system with the control neurons. Analysis revealed the spike-like mixed feedback controller to be a reliable feedback source. Next, coupling two motor neuron allowed the system to reach symmetrical oscillation with greater amplitude. The final step was to allow a control on this amplitude oscillation with great energy efficiency.

But, in my opinion, this thesis only opens the subject of control and many question can still be answered. Firstly, an interesting addition to this work would be to interconnect multiple pendulum by their controllers to try generate different gaits patterns between pendulum. Another step after reaching those gaits would be to try to switch dynamically between them in a smooth way to avoid unnatural and abrupt transitions.

On another point, the controller proposed here relies heavily on a very strong sensory feedback. An interesting challenge would be to use a very weak feedback but try to use neuromodulation to adapt the natural frequency of the HCO to match the frequency of the pendulum. Keeping the already existing neuromodulation for amplitude control in this system would also be very interesting.

Also, the performances of the controller are only discussed in comparison with itself and some natural control criteria. It would be useful to compare this controller to more classical approaches such as the PID. Natural comparison would be the tracking of the reference but also the amount of energy or force used. This would solidify the usefulness of this controller.

Bibliography

- [1] A. Cangelosi, J. Bongard, M. H. Fischer, and S. Nolfi. Embodied intelligence. In J. Kacprzyk and W. Pedrycz, editors, *Springer Handbook of Computational Intelligence*, pages 697–714. Springer Berlin Heidelberg, Berlin, Heidelberg, 2015.
- [2] A. Franci, G. Drion, and R. Sepulchre. Robust and tunable bursting requires slow positive feedback. *Journal of Neurophysiology*, 119(3):1222–1234, 2018.
- [3] S. Grillner. Biological pattern generation: The cellular and computational logic of networks in motion. *Neuron*, 52(5):751–766, 2006.
- [4] A. Hodgkin, A. Huxley, and B. Katz. Ionic currents underlying activity in the giant axon of the squid. *Arch. Sci. Physiol.*, 3:129–150, 1949.
- [5] A. L. Hodgkin and A. F. Huxley. A quantitative description of membrane current and its application to conduction and excitation in nerve. *The Journal of physiology*, 117(4):500, 1952.
- [6] H. Lodish, A. Berk, P. Matsudaira, C. A. Kaiser, M. Krieger, M. P. Scott, L. Zipursky, and J. Darnell. *Molecular Cell Biology*. WH Freeman and Company and Sumanas, Media Connected, 4th edition, 1999.
- [7] E. Marder and D. Bucher. Central pattern generators and the control of rhythmic movements. *Current Biology*, 11(23):R986–R996, 2001.
- [8] R. Sepulchre, G. Drion, and A. Franci. Excitable behaviors. In R. Tempo, S. Yurkovich, and P. Misra, editors, *Emerging Applications of Control and Systems Theory: A Festschrift in Honor of Mathukumalli Vidyasagar*, pages 269–280. Springer International Publishing, Cham, 2018.
- [9] A. A. Sharp, F. K. Skinner, and E. Marder. Mechanisms of oscillation in dynamic clamp constructed two-cell half-center circuits. *Journal of Neurophysiology*, 76(2):867–883, 1996.
- [10] V. A. Straub. Central pattern generator. In M. D. Binder, N. Hirokawa, and U. Windhorst, editors, *Encyclopedia of Neuroscience*, pages 650–654. Springer Berlin Heidelberg, Berlin, Heidelberg, 2009.

- [11] B. Vazifehkhah Ghaffari, M. Kouhnnavard, and S. Elbasiouny. Mixed-mode oscillations in pyramidal neurons under antiepileptic drug conditions. *PLoS One*, 12(6):e0178244, 2017.

Appendix A

Signal Analysis Algorithms